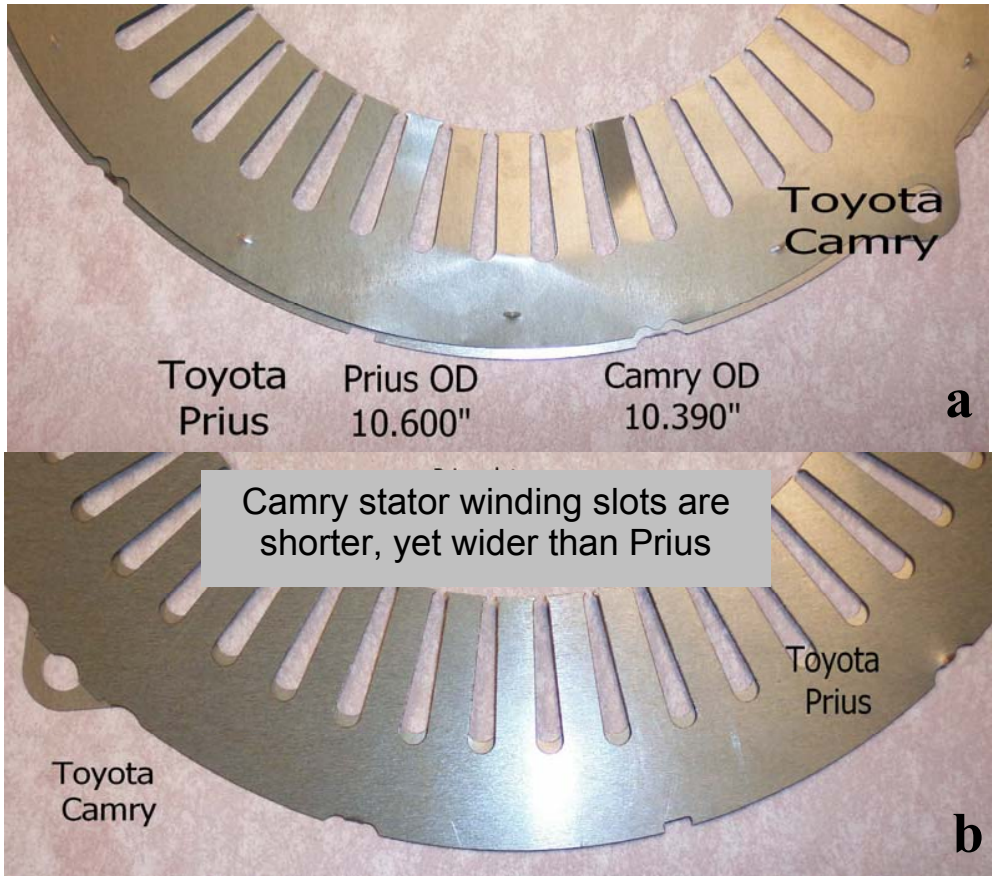

Fig. 2.66. Camry and Prius motor stator laminations.

Figure 2.67 shows details of the Camry rotor assembly and the "V" orientation of the neodymium iron boron (NdFeB) interior PM. Looking at the pair of magnets in the foreground, it is possible to see the narrow support bar that passes between them. This support bar, missing from the Prius motor laminations, helps to enable the motor to operate at much higher rotational speeds.

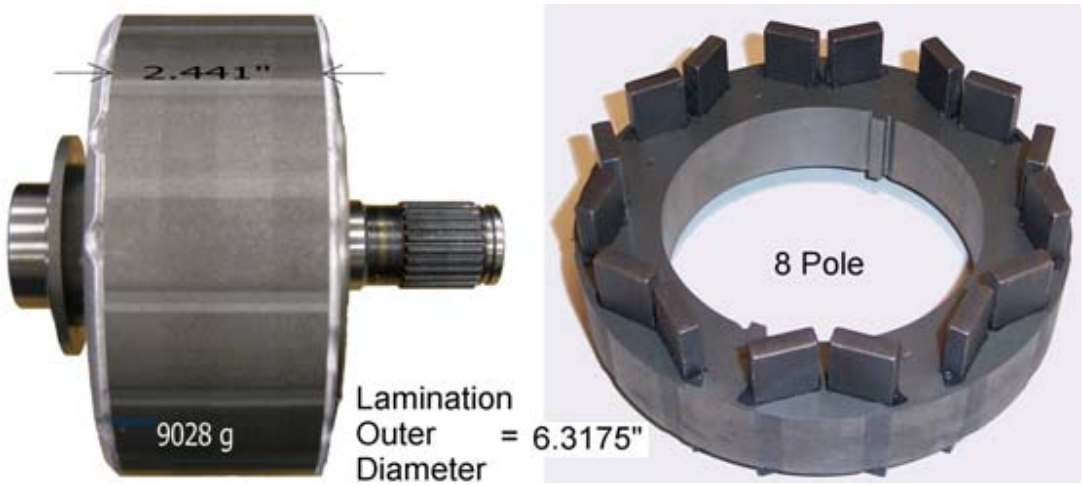

Fig. 2.67. Camry rotor assembled (left) and partially disassembled (right).

In making various comparisons between the Camry and Prius motor components, the highlights shown in Table 2.8 were generated. The table summarizes the general motor design, rotor and stator dimensions/mass, and the wiring and slot details of the stator. Because the rotor and stator lamination geometries are difficult to fully describe in a table, Figs. 2.68 and 2.69 provide this information. The length of the magnets decreased along with the decrease in the stator and rotor lamination stack length. However, the thickness and width of the Camry and Prius motor PMs are very similar. Details regarding the magnet characteristics are provided in Section 2.2.4. Various motor characteristics were experimentally measured and the results are presented in Section 3.

Table 2.8. 2007 Camry/2004 Prius motor design comparison highlights

Parameter	Camry	Prius	Comments
Lamination Dimensions			
Stator OD, mm	264	269	OD
Stator ID, mm	161.93	161.93	ID
Stator stack length, cm	6.07	8.4	
Rotor OD, mm	160.47	160.47	OD
Rotor lamination ID, mm	105	111	ID
Rotor stack length, cm	6.2	8.36	
Air gap, mm	0.73025	0.73025	
Lamination thickness, mm	0.31	0.33	
Mass of Assemblies			
Rotor mass, kg	9.03	10.2	Including rotor shaft.
Stator mass, kg	18.0	25.9	
Stator core mass, kg	12.38	19.05	Laminations only.
Stator Wiring			
Number of stator slots	48	48	
Stator turns per coil	14	9	
Parallel circuits per phase	2 legs	0	
Turns in series per phase	4 per leg	8	
Number of wires in parallel	9 per leg	13	
Wire size, American wire gauge (AWG)	20	19	
Phase resistance at 21°C, ohm	0.023	0.069	Average of phase-to-phase divided by two.
Total mass of stator copper, kg	5.6	6.8	
Slot depth, mm	30.9	33.5	
Slot opening, mm	1.88	1.93	
Casing			
Motor casing mass, kg	9.5	8.9	Camry has thicker walls, larger heat exchanger, speed reduction gear casing and bearings
Motor casing diameter, cm	30.2	29.9	
Motor casing axial length, cm	17.0	20.5	
Magnets (NdFeB)			
Magnet dimensions, mm	60.6×19.1×6.6	83.1×18.9×6.5	One magnet (1/2 of "V" or pole).
Magnet volume, cm^3	7.63	10.2	One magnet (1/2 of "V" or pole).
Magnet mass, grams	58	77	One magnet (1/2 of "V" or pole).
Total mass of magnets, kg	0.928	1.232	Entire magnet mass in rotor.

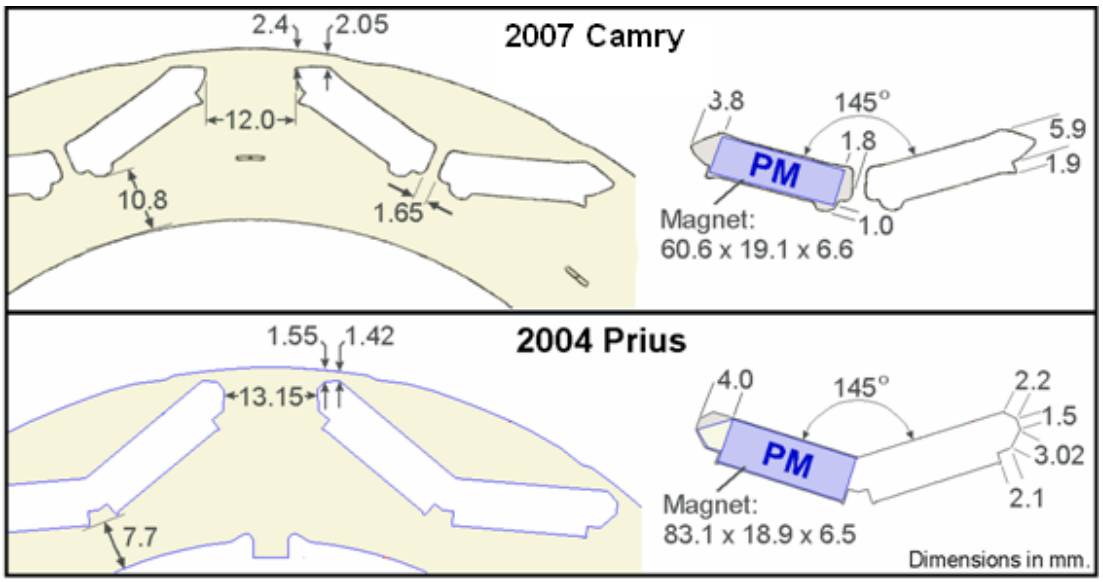

Fig. 2.68. Camry and Prius motor rotor lamination/PM design.

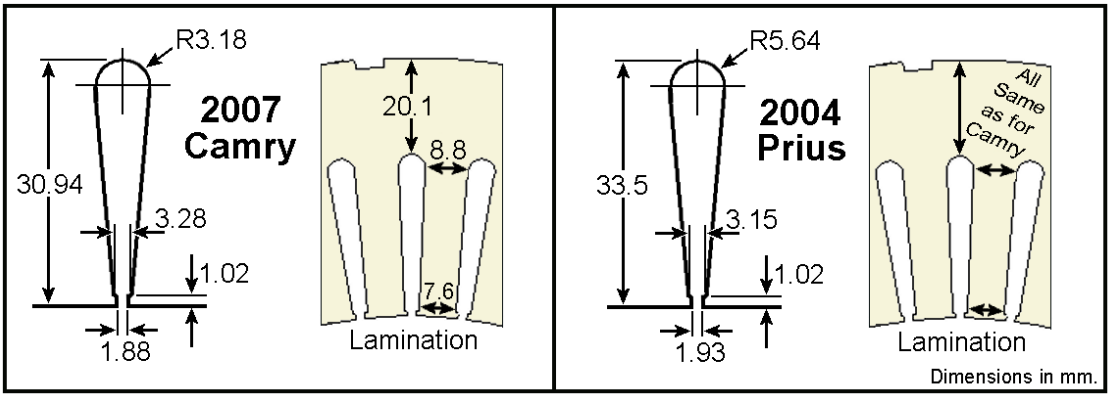

Fig. 2.69. Camry and Prius motor stator lamination/slot design.

Volume assessments of the Camry generator housing were conducted with the general approach and calculations shown in Fig. 2.70. The total volume of the Camry generator housing is about 11 L and the total mass is about 28 kg. The power rating of the Camry generator is approximately 40 kW compared to the 33 kW rating of the Prius generator. Comparisons of the Camry and Prius generator stators and rotors are provided in Figs. 2.71 and 2.72, respectively. It is evident that the generator has increased in both diameter and stack length by about 14% and 17.5%, respectively. The size of the Camry generator is more suited for continuous operation. A thermistor is embedded within the stator windings to provide temperature feedback and the MG ECU will discontinue operation of the generator upon reaching an over-temperature condition. A summary and comparison of the Camry and Prius generator specifications is provided in Table 2.9.

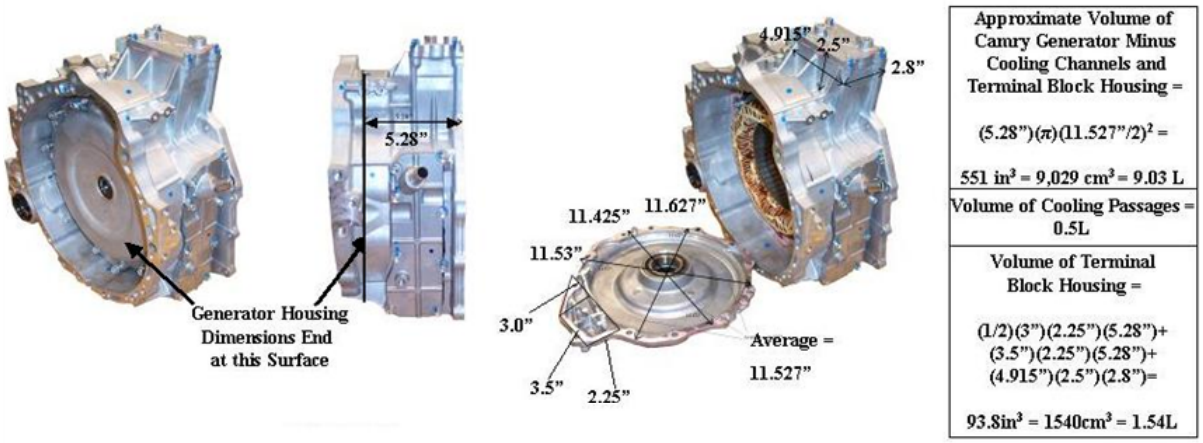

Fig. 2.70. Camry generator volume assessment.

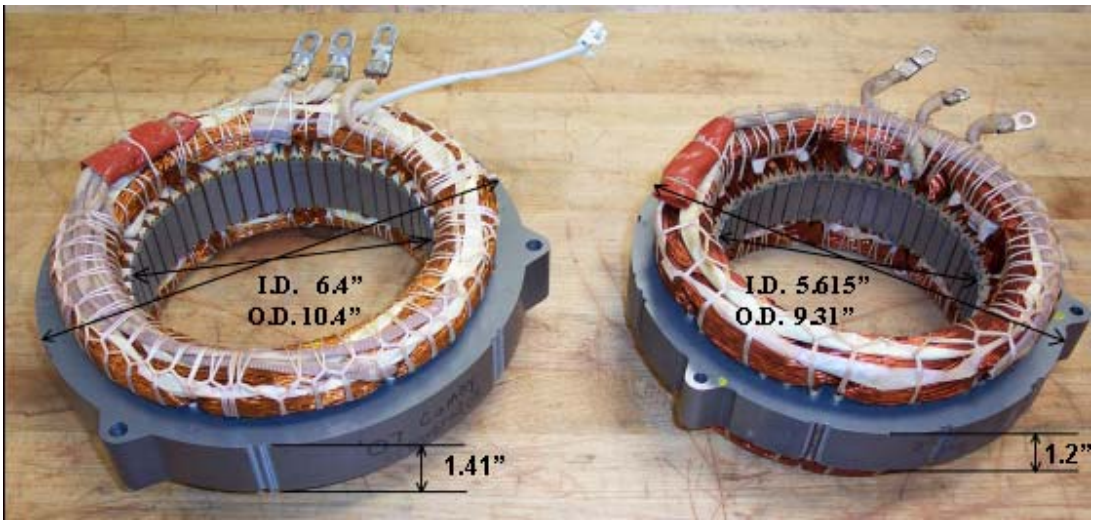

Fig. 2.71. Camry (left) and Prius (right) generator stator comparison.

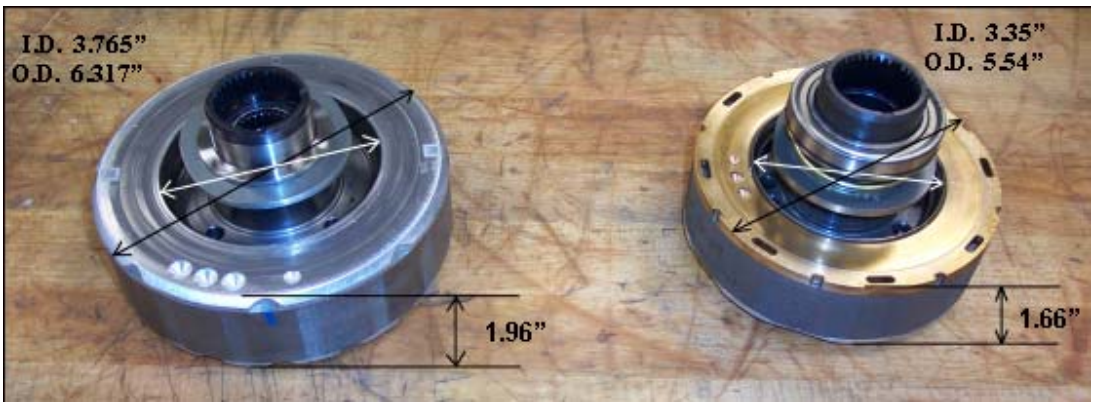

Fig. 2.72. Camry (left) and Prius (right) generator rotor comparison.

Table 2.9. 2007 Camry/2004 Prius generator design comparison highlights

Parameter	Camry	Prius	Comments
Lamination Dimensions			
Stator OD, mm	264.16	236.2	
Stator ID, mm	162.6	142.6	
Stator stack length, cm	3.58	3.05	
Rotor OD, mm	160.46	140.72	
Rotor lamination ID, mm	95.63	85.09	
Lamination thickness, mm	0.31	0.33	
Mass of Assemblies			
Rotor mass, kg	5.188	4.01	Including rotor shaft
Stator mass, kg	12.09	9.16	
Stator Wiring			
Number of stator slots	48	48	
Number of wires in parallel	18	12	
Wire size, AWG	20	20	

2.2.4 PM Characteristic Assessments

Hysteresis tests were conducted on the Camry motor PMs using the Walker Scientific AMH-40 hysteresisgraph (shown in Fig. 2.73), which is capable of producing 30,000 Oersteds of magnetic field strength. A hysteresis test provides information regarding the remanent flux density and coercivity of a magnet and these tests are often conducted over a wide range of temperatures. The remanent flux density, B_r, is the remaining flux density created by the magnet with no external field applied. Or simply stated the remanent flux density represents the strength of the magnet. The remanent flux density decreases to some extent with increasing temperature. The coercivity of a magnet is defined to be the intensity of the magnetic field required to reduce the magnetization of the magnet, and the coercivity of a magnet decreases with increasing temperature. Coercivity is an especially important characteristic of PMs that are used in HEV applications, which often involve high temperature and high field weakening operation conditions.

During hysteresis tests, the magnet is subjected to positive and negative magnetic fields while the impact of the externally applied magnetic field on the magnet is observed. A graph from hysteresis tests conducted on a magnet from the Camry motor rotor at 110ºC is shown in Fig. 2.74. Two curves are shown on the graph with the burgundy trace being the normal, or total magnetic flux density, and the turquoise trace representing the intrinsic magnetic flux density. The intrinsic flux density is the flux density solely created by the magnet, which is obtained by subtracting the applied flux density from the total flux density. The remanent flux density is the value at which both curves intersect with the y-axis, which is at y = 11.86 kG in this case. The value of coercivity is found at the point where the intrinsic curve crosses the x-axis, which is x = 14.46 kOe in this case. A similar graph is provided in Fig. 2.75, with the hysteresis evaluation conducted at an ambient temperature of 198ºC. Notice that the curves are much closer to the origin when compared to Fig. 2.74. As the temperature increased from 110–198ºC, the remanent flux density and coercivity decreased from 11.86–10.29 kG and 14.46–5.757 kOe, respectively. The drastic decrease of the coercivity indicates that the magnet is much more susceptible to demagnetization at high temperatures.

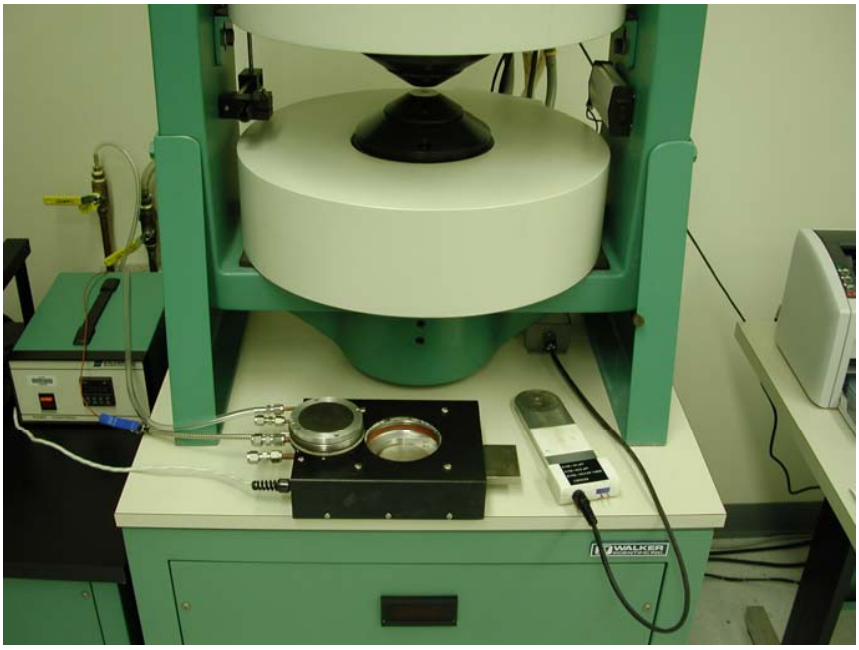

Fig. 2.73. Walker Scientific hysteresis graph.

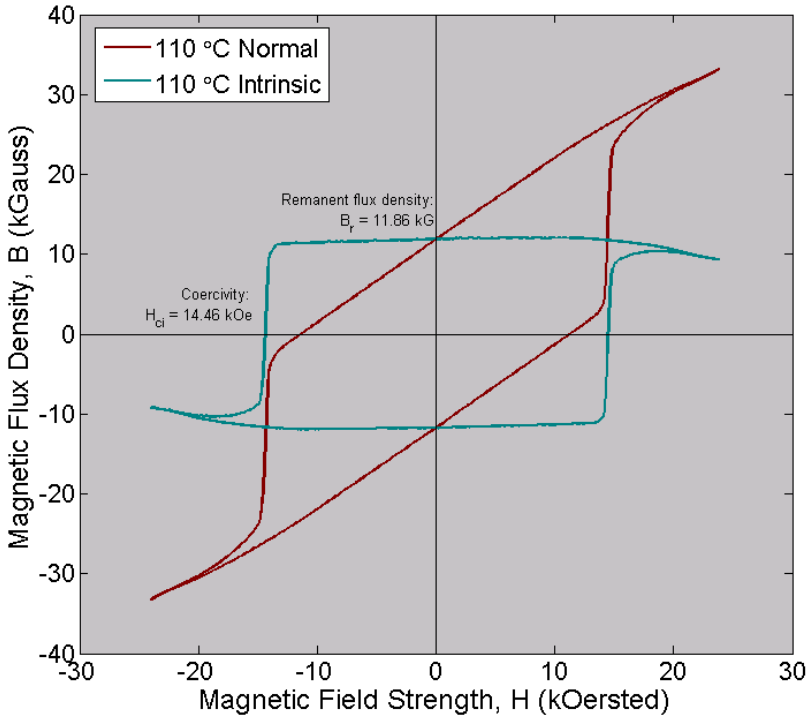

Fig. 2.74. Hysteresis graph for Camry motor magnet at 110°C.

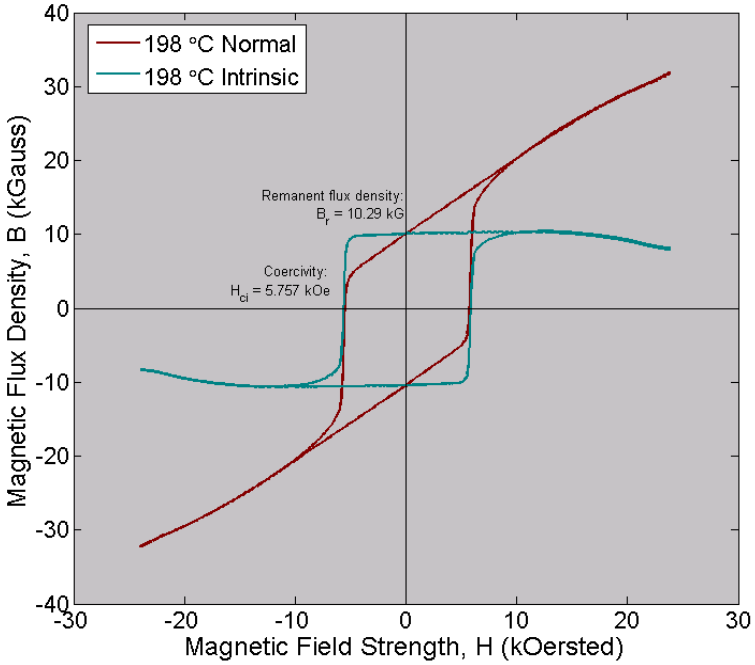

Fig. 2.75. Hysteresis graph for Camry motor magnet at 198ºC.

Intrinsic curves from hysteresis tests conducted with a Camry motor magnet at various temperatures have been combined onto one plot in Fig. 2.76. These curves further exemplify the diminishing nature of the remanent flux density and coercivity with increasing temperature. A similar graph containing the intrinsic curves obtained from the Prius motor magnet hysteresis tests is provided in Fig. 2.77. Although it is difficult to make a detailed comparison using these figures, a general comparison indicates that the coercivity of the Camry magnet is significantly lower than that of the Prius.

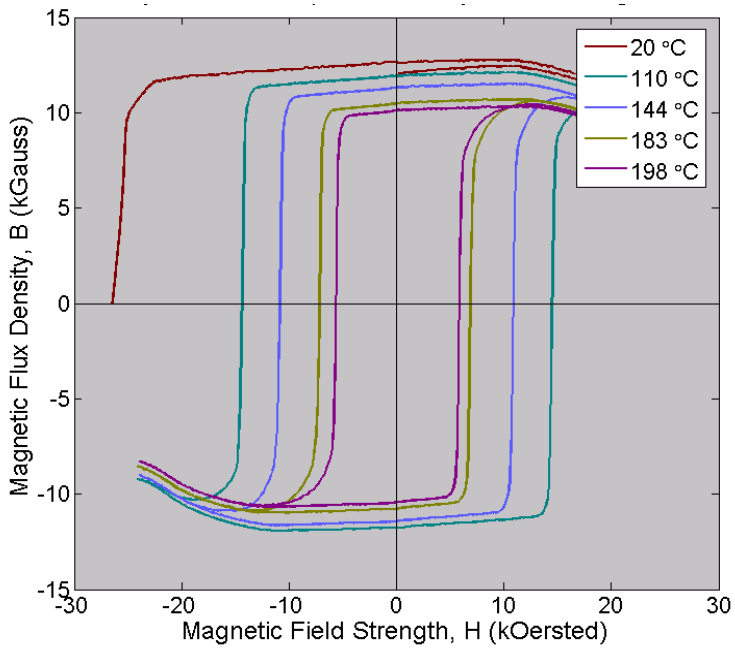

Fig. 2.76. Intrinsic hysteresis graphs for Camry motor magnet at various temperatures.

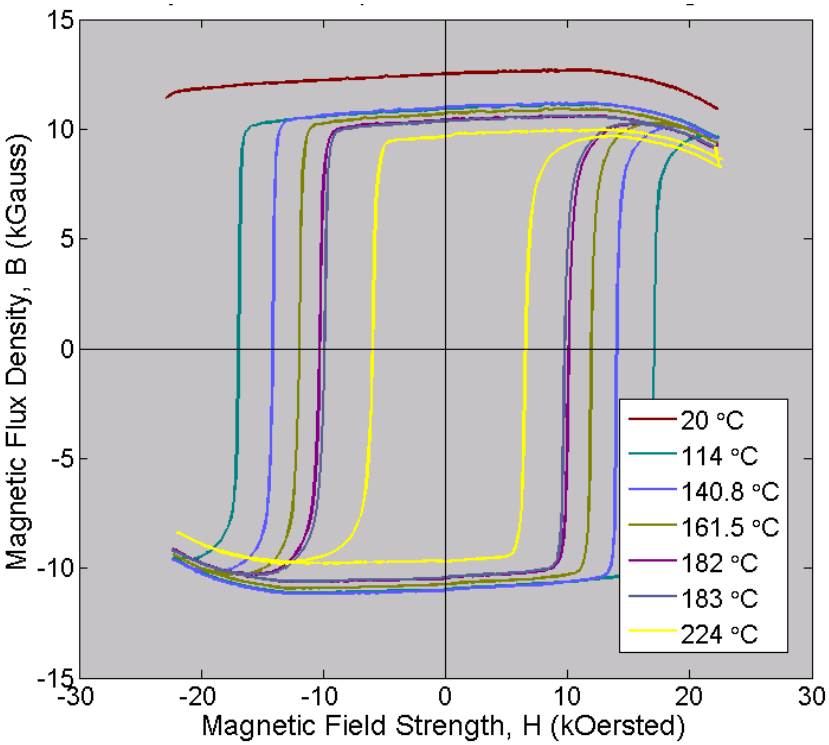

Fig. 2.77. Intrinsic hysteresis graphs for Prius motor magnet at various temperatures.

To provide a more straight forward comparison of the remanent flux density characteristics of the Camry and Prius motor magnets, the values were plotted versus temperature in Fig. 2.78. The strength of the Camry motor magnet is marginally higher than the strength of the Prius motor magnet, except for temperatures beyond about 215ºC. A similar plot is shown in Fig. 2.79 for the coercivity versus temperature relationship of the Camry and Prius motor magnets. The coercivity of the Camry motor magnet is about 70% of the coercivity of the Prius magnet, except for temperatures above about 200ºC where the coercivity values are a bit closer.

Although the Camry motor magnet is slightly stronger than the Prius magnet, the coercivity is much lower and, therefore, is much more susceptible to demagnetization when subjected to high temperatures and/or high strength magnetic fields which oppose the direction of the magnetic field of the magnet. It is common to apply opposing magnetic fields to the magnets when operating at high speeds, wherein high back-emf voltages are subdued to enable high speed operation within the voltage constraints. It is very likely that the cost of the Camry motor magnet is lower than the cost of the Prius magnet and although it has a lower coercivity, demagnetization can be avoided using preventative control techniques.

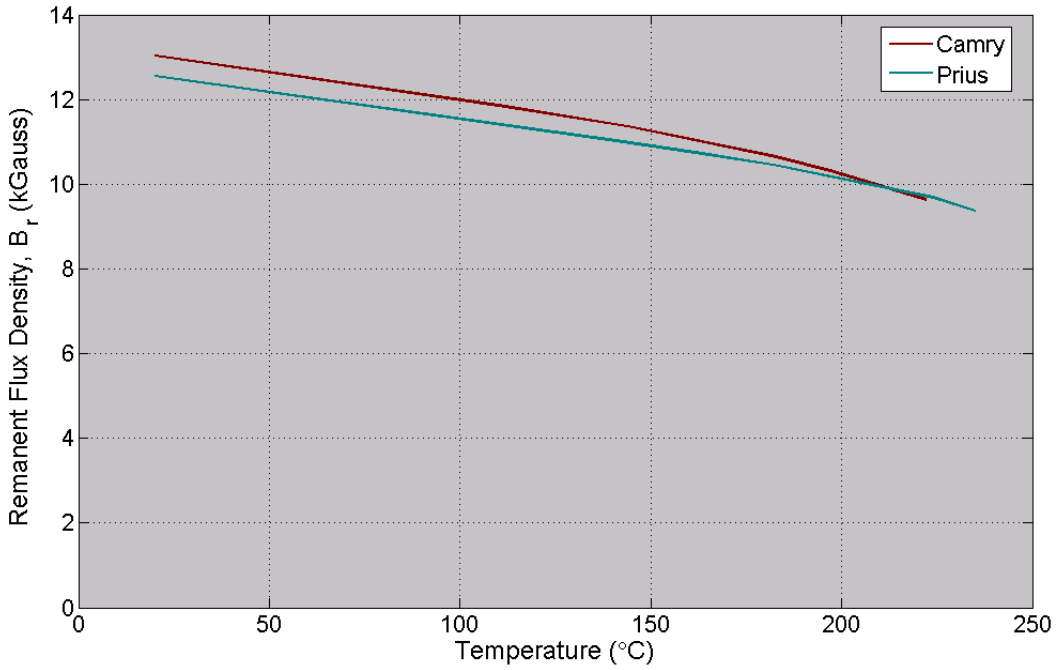

Fig. 2.78. Remanent flux density for Camry and Prius motor magnet.

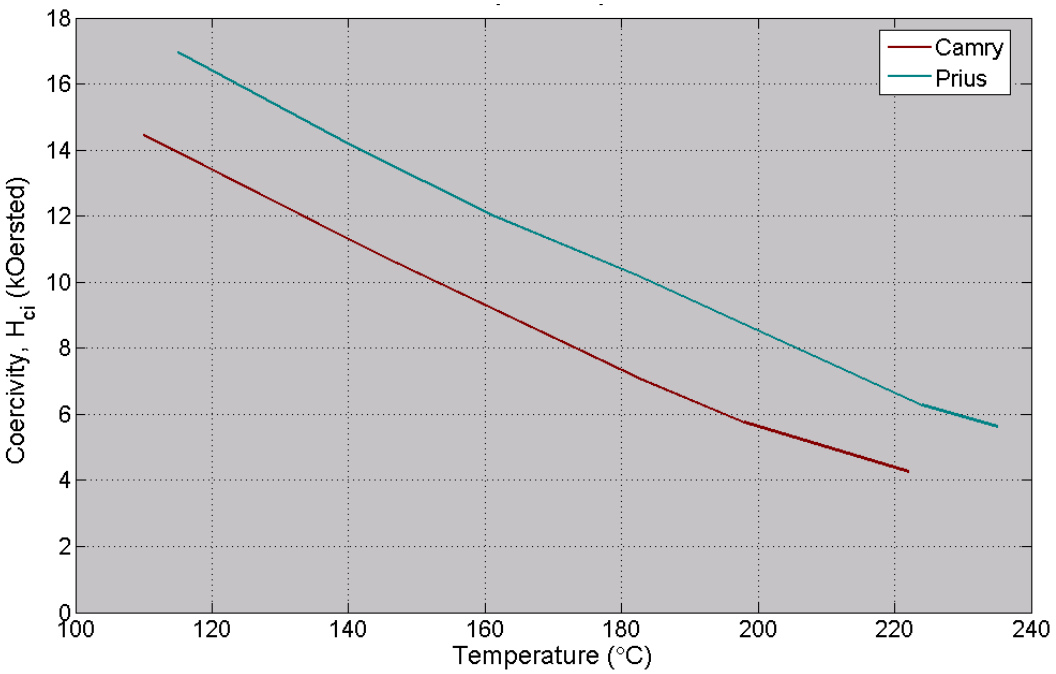

Fig. 2.79. Coercivity of Camry and Prius motor magnet.

3. BENCHMARKING TESTS OF CAMRY PMSM AND INVERTER

This section describes the hybrid Camry subassembly preparation and the back-emf, rotational loss, locked-rotor, performance/efficiency, and continuous load duration tests. With the exception of the back-emf, rotational loss, and locked-rotor tests which did not require inverter operation, each was performed using both the PMSM and inverter subsystems.

3.1 SUBSYSTEM PREPARATION FOR TESTING

As design and packaging assessments of the transaxle and PCU were being conducted, preparation for testing of the subsystems was commenced, including hardware design and fabrication, controller/interface development, and instrumentation for the DAQ. Two separate approaches were taken to adapt the Camry PMSM to separate dynamometer setups as each provided a benefit in terms of implementation time versus unmitigated testing capability. Although basic framework was available from previous benchmarking efforts, a large portion of the efforts devoted to controller/interface and DAQ development required innovation.

3.1.1 Hardware Preparation

The first test setup approach provided a quick resolution and means to initiate testing, yet it did not provide testability throughout the entire operation range of the PMSM. Therefore, while the initial tests were being conducted with the first test setup, a second approach was instituted. Additionally, the dynamometer test cell was upgraded to suit the high speed and power demands of the Camry PMSM.

Similar to the approach taken with the Prius transaxle hardware setup, the first approach involved welding the power split planetary gear as shown in Fig. 3.1. This causes the ICE input shaft, which is easily accessible, to rotate at the same speed as the ring gear of the power split planetary gear unit. For the Prius design, the ring gear rotates at the same speed of the primary drive motor, MG2. However, the MG2 of the Camry is connected to the ring gear through the speed reduction planetary gear unit. Thus, although the first approach provided a quick means to access the motive force of the motor, uncertainties were associated with the influence of speed reduction gear losses upon power and efficiency measurements. To obtain accurate motor efficiency measurements, it is crucial to accurately measure the mechanical power produced directly by the motor. Nonetheless, the setup provided a quick means of test initiation and valuable insights, such as controller development aspects. Additionally, the setup eliminated the immediate need for equipment with high speed testing capabilities, which was not installed until a later time during the project duration.

The second approach involved design and fabrication of a shaft and faceplate (shown in Fig. 3.2) which adapts to the Camry motor rotor, transaxle mounting pattern, and the high speed torque cell face mount and spline shaft. Design considerations were carefully surmised to ensure that no part of the system operation was hindered or enhanced. Particularly, intense focus was placed on maintaining the operational characteristics of the thermal management and lubrication system mostly by ensuring that the oil flow pattern throughout the transaxle remained unchanged. This approach avoids uncertainties associated with the losses of the high speed reduction gear, thereby providing accurate measurements of motor power output.

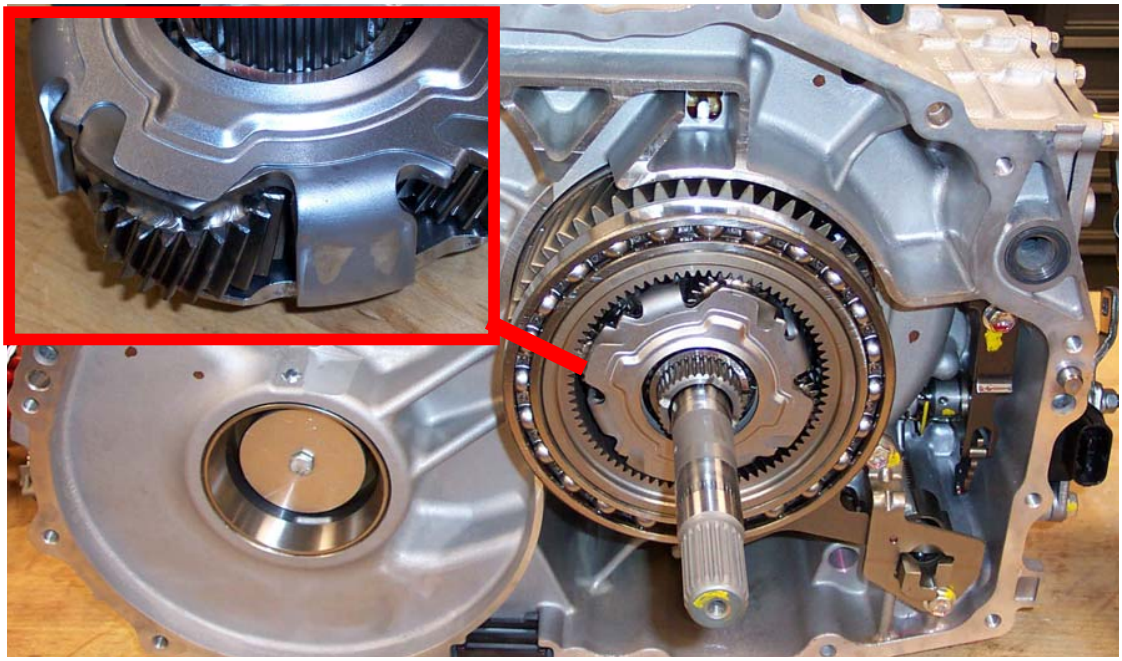

Fig. 3.1. First test setup approach with welded Camry planetary gear.

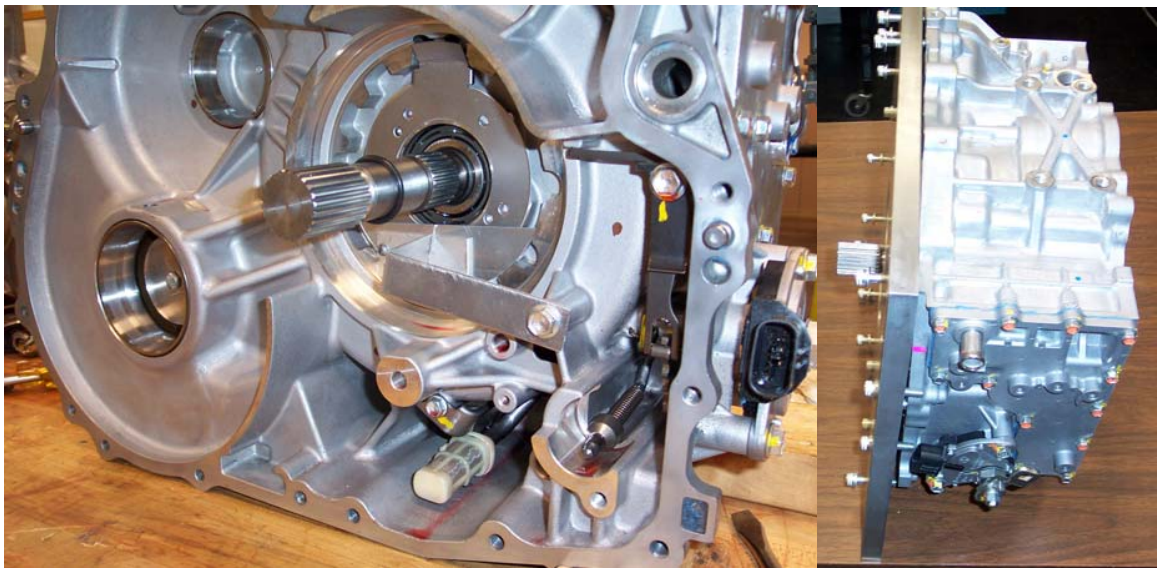

Fig. 3.2. Second test setup approach with modified motor rotor shaft.

To accommodate the high speed and power testing requirements of the Camry PMSM, the test cell was upgraded with a 400 hp dynamomter and speed reduction gearbox, as shown in Fig. 3.3. The speed reduction gearbox was required to match the speed range of the dynamometer to a speed of up to 18,000 rpm on the high speed input shaft. A high speed torque transducer (not shown) attaches to the high speed input shaft of the gearbox via a face mount support. The spline shaft output of the modified Camry rotor shaft and the fabricated faceplate mates with the input of the high speed torque transducer.

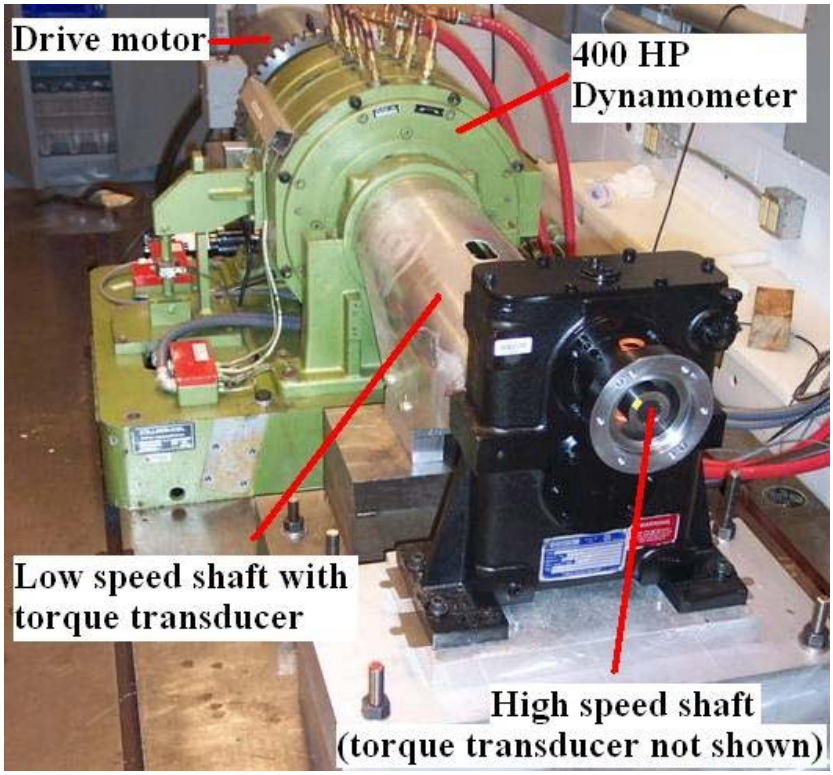

Fig. 3.3. Upgraded dynamometer test cell.

3.1.2 Instrumentation and DAQ Development

The PCU, PMSM, and transaxle were instrumented with thermistors and TCs in order to monitor and record thermal conditions and characteristics of the subsystem during various operation conditions. In preparation for performance, efficiency, and continuous duration tests in the ORNL laboratory, the motor inverter was instrumented with three TCs placed in the edges of the three power electronics heat spreaders as shown in Fig. 3.4. Two other TCs were placed in the (1) aluminum wall against the potted inductor of the buck/boost converter, and (2) edge of the heat spreader for the buck/boost converter power electronics module.

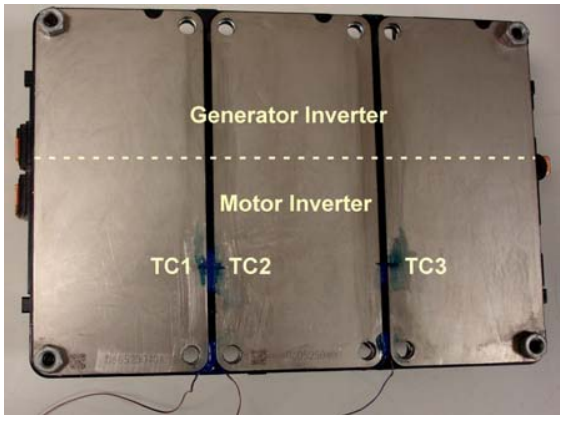

Fig. 3.4. TCs in the inverter power electronics heat spreaders.

Thermistors were installed in various locations on the stator windings and transaxle housing, as indicated in Fig. 3.5. Each location has a unique letter identifier and additional location information. For example, thermistor "D: ML 1" is located on the motor lead side of the stator at the 1 o'clock position indicated by the red circle. All thermistor locations on the front side of the stator are indicated by red circles and thermistor locations on the rear of the stator are marked with cyan circles. Case thermistor locations are indicated by light green circles and oil thermistor locations are indicated by orange circles. Note that thermistor "E: ML 2" is the original factory installed thermistor. The resistance of an identical thermistor was evaluated over a wide range of temperatures in order to generate a lookup table to be used with the DAQ software.

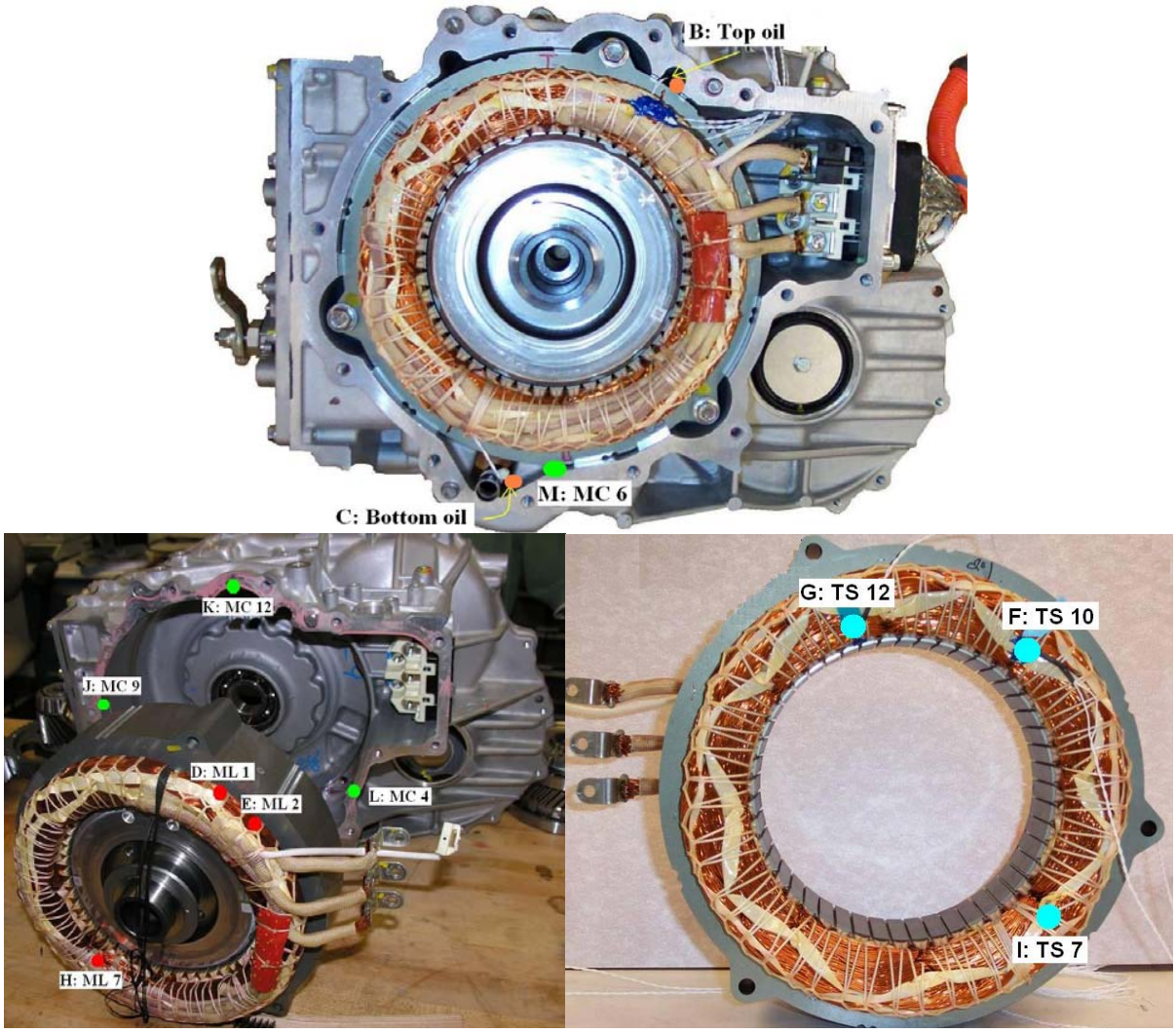

Fig. 3.5. Thermistor locations on PMSM and transaxle.

The Camry transaxle was modified to include windows and temporary viewports in the locations shown in Fig. 3.6 to facilitate observations of the oil system characteristics. These observations provided useful information regarding oil circulation and oil levels in various locations throughout the transaxle. It was especially necessary to assess these characteristics as the design, fabrication, and implementation of the second test setup approach was carried out and that these characteristics remained unchanged during

operation. It was determined that the oil reservoirs as well as the upper oil channels are nearly full when the ring gear is rotating at speeds near 1,000 rpm.

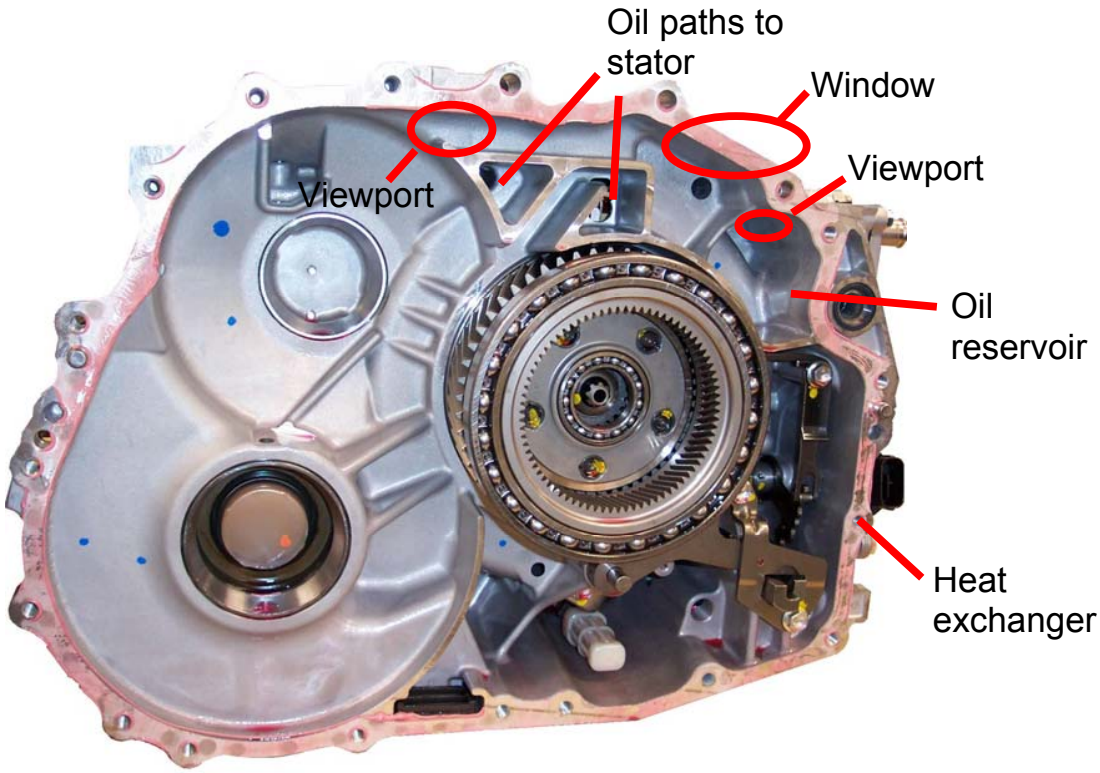

Fig. 3.6. Viewport and window locations implemented on transaxle.

A program written in the Visual Basic programming language was developed to collect data from various measurement instruments and merge the data into a convenient spreadsheet format. Torque, speed, and mechanical power were obtained using a Himmelstein torque and speed transducer. Temperature measurement signals from thermistors and TCs were collected with a Keithly 2700 acquisition unit. A Yokogawa PZ4000 power analyzer was used to carry out electrical measurements such as ac and dc rms voltage, rms current, real power, and many other properties of the waveforms.

The DAQ system was important not only for data logging, but it also served as a real time feedback system in which system conditions were monitored to ensure that operational limitations were not violated and to ensure that the system was being operated in an optimal manner. Temperature and current constraints were the primary limitations of the entire drive system. Efficiencies were calculated using the mechanical and electrical data and were used to verify that the controller operation was optimized.

3.1.3 Controller and Interface Development

The hybrid subsystems of the 2007 Toyota Camry were evaluated for performance and efficiency characteristics such as peak and continuous power ratings and motor/inverter efficiency. Continuous operational capabilities are greatly affected by the heat transfer characteristics of the motor, which is cooled through oil circulation and an ethylene-glycol coolant loop. The hybrid subsystems were operated over a broad torque-speed range in order to collect and analyze thermal and electrical data at a multitude of operation points. For each operation point during efficiency evaluations, the system was held in steady state for at least 20 seconds as a minimum of 5 data samples were taken.

ORNL's dynamometer test cell and Opal-RT-based speed and current feedback controller were adapted to provide the torque needed at each reference speed. Thus, as the applied torque from the dynamometer was varied manually, the controller regulated the torque producing current appropriately. The current controller consists of two standard proportional-integral (PI) controllers for the direct and quadrature currents, i_d and i_q, respectively. These *d-q* components are obtained by applying the *d-q* transformation to the three-phase currents which have a fixed reference. The transformation converts the three-phase currents into two-phase vectors, which have a reference that rotates with the rotor. Therefore, precise rotor position feedback is used during this transformation.

The steady state torque equation for the salient PM machine is expressed by:

$$\tau_L = n_p(L_d - L_q)\, i_d i_q + n_p K i_q , \tag{1}$$

where

n_p is the number of pole pairs,
L_d is the *d-axis* inductance,
L_q is the *q-axis* inductance, and
K is the back-emf and torque-current factor.

The total torque given by Eq. (1) consists of two torque terms which are reluctance torque and PM torque, respectively. PM torque is produced only by the current component along the *q-axis*. If current is applied which results with a negative component along the *d-axis*, positive reluctance torque is developed since the difference, L_d-L_q, in the first term is negative and all remaining variables and constants are positive in the motoring region. In theory, there is an infinite amount of *d-q* current combinations that will satisfy a particular operation condition. There is an optimal *d-q* current combination in which the motor efficiency is maximized for each particular torque. It is difficult to determine the optimal current trajectories for the entire torque-speed range, as complex factors such as effects of saturation and harmonics must be considered. Therefore, the DAQ was used to monitor the system efficiency to ensure that the controller is operating optimally.

A high level diagram of the Opal-RT controller and interface system is shown in Fig. 3.7. A console personal computer (PC) is used to develop and modify control schemes in a block diagram format, which is converted and compiled to traditional programming languages (mostly C) and sent to the target nodes through an ethernet network. The target nodes execute the controller code in real time and the console PC is used to control the mode of the controller operation as well as to update various parameters if desired. While the development process is more straightforward than microprocessor programming, the PC based architecture of the target nodes introduces a significant degradation in terms of control sampling frequency. Therefore, the system resources must be utilized in an efficient manner.

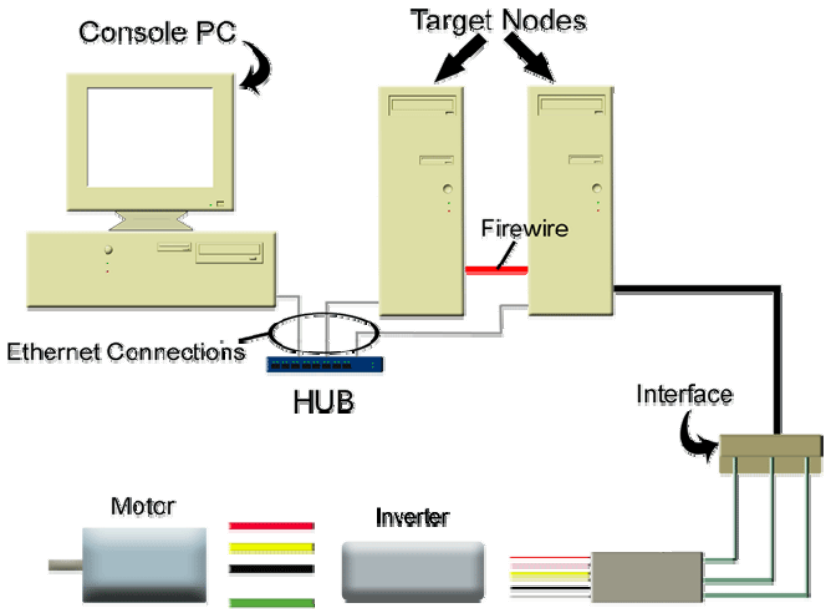

Fig. 3.7. Opal-RT controller and interface system.

3.2 BACK-EMF TEST RESULTS

The non-energized Camry PMSM was spun at various speeds over its full design range to obtain back-emf data. The shaft speed and back-emf data (line-to-neutral rms averaged for the three phases) is plotted in Fig. 3.8. This test was repeated after the performance/efficiency mapping test to verify that no magnetic strength was lost in the rotor during performance tests or extended periods of high-temperature testing. As expected, there were no significant differences in the data obtained from the second back-emf test.

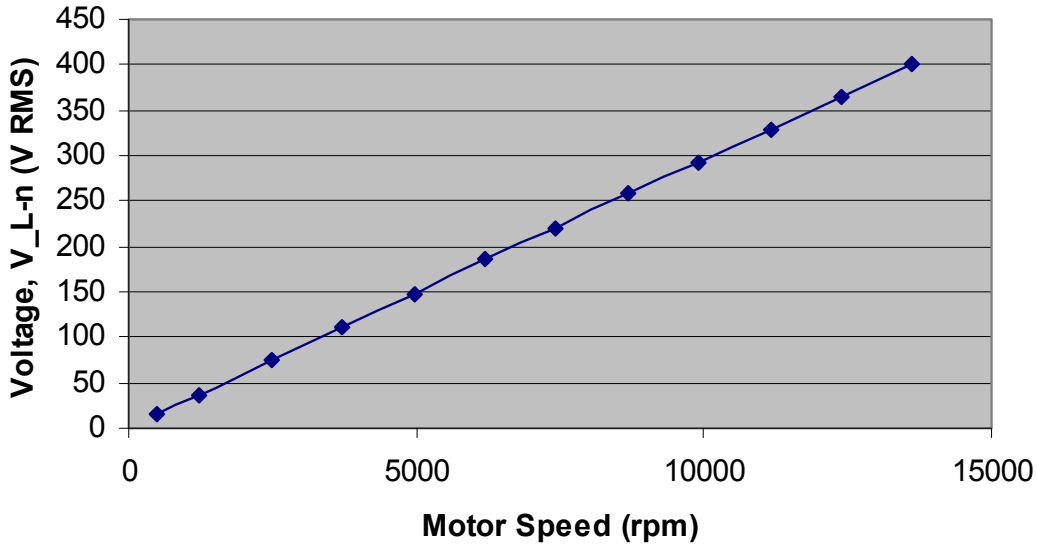

Fig. 3.8. 2007 Camry motor back-emf test results.

A plot containing the line-to-neutral back-emf voltage measurements observed during benchmarking evaluations of the Prius is shown in Fig. 3.9. A comparison of Figs. 3.8 and 3.9 indicates that the volts-per-hertz ratio of the Prius back-emf is higher. However, the maximum back-emf voltage of the Camry, observed at a shaft speed of 14,000 rpm is much higher than the maximum back-emf voltage of the Prius at 6,000 rpm. Note that the ratio of these maximum voltages is approximately equal to the ratio of the maximum dc-link voltages, which is 650/500.

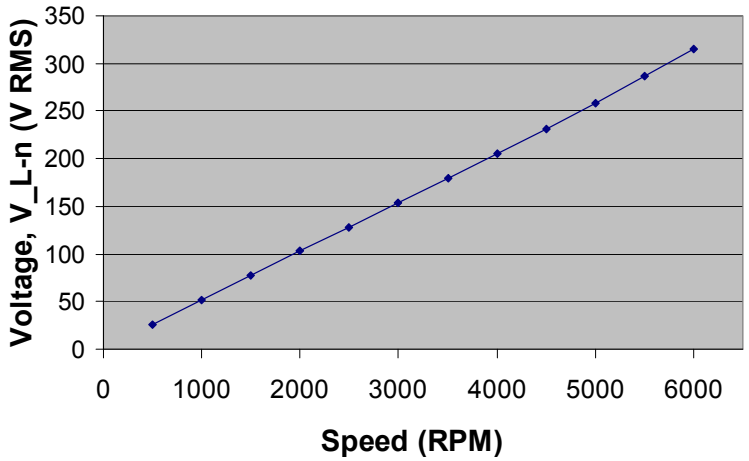

Fig. 3.9. 2004 Prius motor back-emf test results.

3.3 ROTATIONAL LOSS ASSESSMENTS

The rotational losses of the entire gear train and the Camry motor alone were evaluated by rotating the input shafts with an external drive motor. Gear train loss assessments began with the entire gear system installed, which includes the drive gears and planetary gears. The generator and motor rotor were removed in order to assess only the gear losses and motor core loss assessments were conducted at a later time. Torque and power measurements were measured and plotted versus ring gear speed as shown in Figs. 3.10 and 3.11, respectively. The average oil temperature was slightly higher than room temperature during these tests. Note the maximum speed shown in this plot is 5,500 rpm and since the speed reduction gear ratio is 2.47, the corresponding motor speed is 13,585 rpm and the vehicle speed associated with this extreme condition is approximately 113 miles per hour.

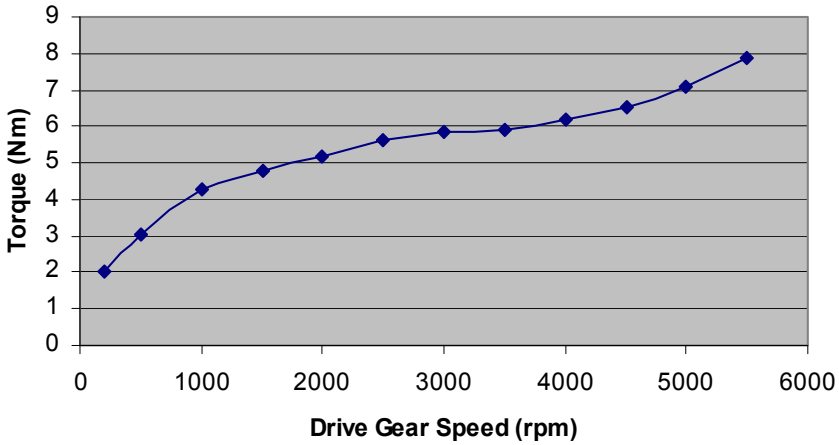

Fig. 3.10. 2007 Camry gear train rotational torque.

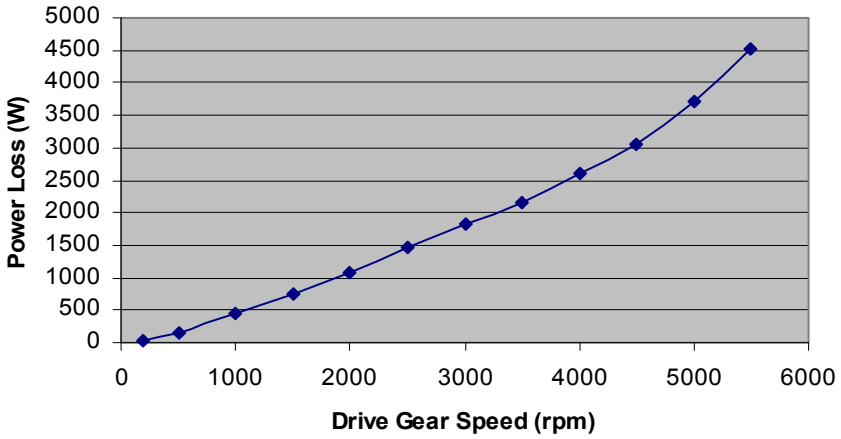

Fig. 3.11. 2007 Camry gear train rotational losses.

Results from the rotational loss tests conducted with the shaft connected directly to the motor rotor are shown in Fig. 3.12. These losses are mostly comprised of core (or iron) losses, which are associated with eddy currents and hysteresis effects. In combining the gear losses shown in Fig. 3.11 and the core losses shown in Fig. 3.12, it is inferred that a significant amount of losses are associated with the rotational motion of the drive system. Nonetheless, these losses are exceptionally low when compared to that of a conventional automatic transmission, which includes multiple planetary gears and clutching mechanisms.

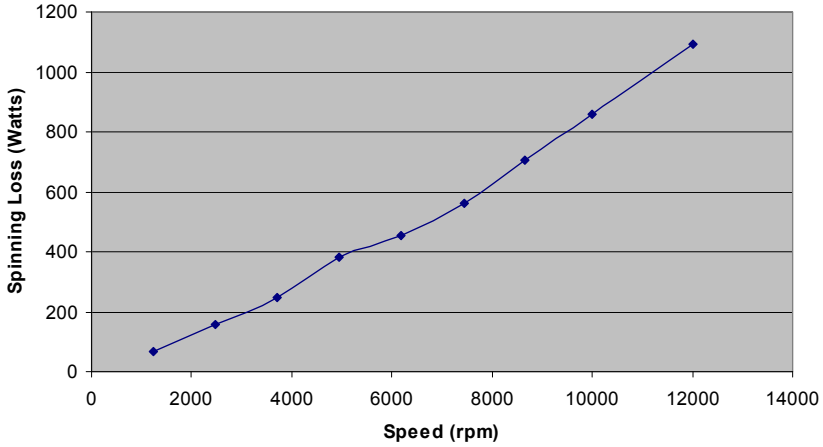

Fig. 3.12. 2007 Camry motor rotational losses.

Further gear loss assessments were conducted to obtain information which more specifically describes the losses associated with each component, as well as the influence of oil temperature upon the gear losses. The first test was conducted with all gears installed and the motor rotor removed and the oil temperature initially low. The Bay-Voltex external coolant temperature regulator was used to increase the oil temperature in order to observe the effects of increasing oil temperature as the rotor speed was held constant. These tests were conducted at ring gear speeds of 2000, 3500, and 5000 rpm. A gear system was removed after each test was conducted, and therefore the associated losses of the removed gear system can be assessed. The results from these tests are shown in Fig. 3.13, with the 2000, 3500, and 5000 rpm traces shown in shades of blue, green, and red, respectively. After tests were conducted with no motor rotor, the drive gears were removed, then the planetary gears were removed. Losses of the entire gear train tend to decrease with increasing oil temperature due to deceasing oil viscosity and losses are minimal near the common operation temperatures of the transaxle, namely 50–80ºC. Extended tests at

3500 rpm reveal that the gear losses increase beyond a temperature of 90ºC. In comparing the loss difference of each of the tests, the drive gears have the highest amount of losses associated with spinning motor and the planetary gears contribute only a small amount.

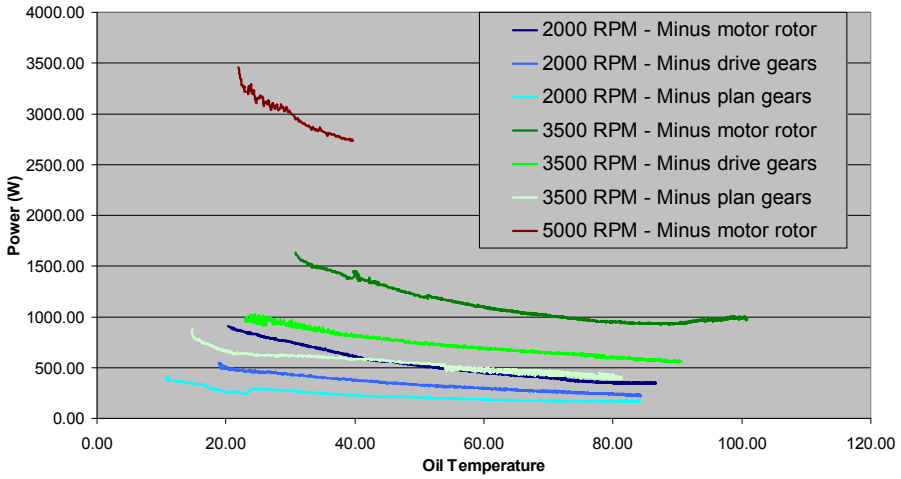

Fig. 3.13. 2007 Camry gear losses vs. oil temperature at various ring gear speeds.

3.4 LOCKED ROTOR TEST

A series of locked rotor tests were performed to determine the torque-producing behavior of the PMSM motor. During locked rotor tests, the rotor is rotated throughout an electrical cycle and the shaft is rigidly locked at each position as dc current is applied. Torque values were obtained from an in-line shaft torque sensor when the motor windings were energized. The resulting data was used to produce torque versus electrical position plots, which are shown in Fig. 3.14 for various current levels. These tests were not conducted at extremely high dc currents to avoid high temperatures which could potentially damage the stator windings or rotor magnets. The peak torque for each current level was chosen and is indicated by the blue trace in Fig. 3.15. Peak locked rotor torques for the Prius are also included in the figure, and are much larger than that of the Camry. However, the equivalent torque of the Camry motor on the low speed side of the speed reduction gear is much higher, as indicated by the yellow trace in Fig. 3.15.

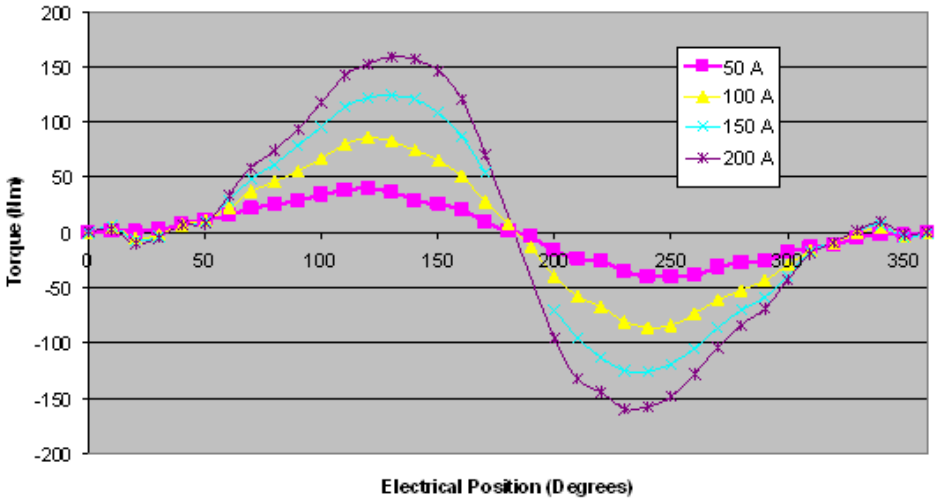

Fig. 3.14. 2007 Camry locked rotor torque vs. position for various dc currents.

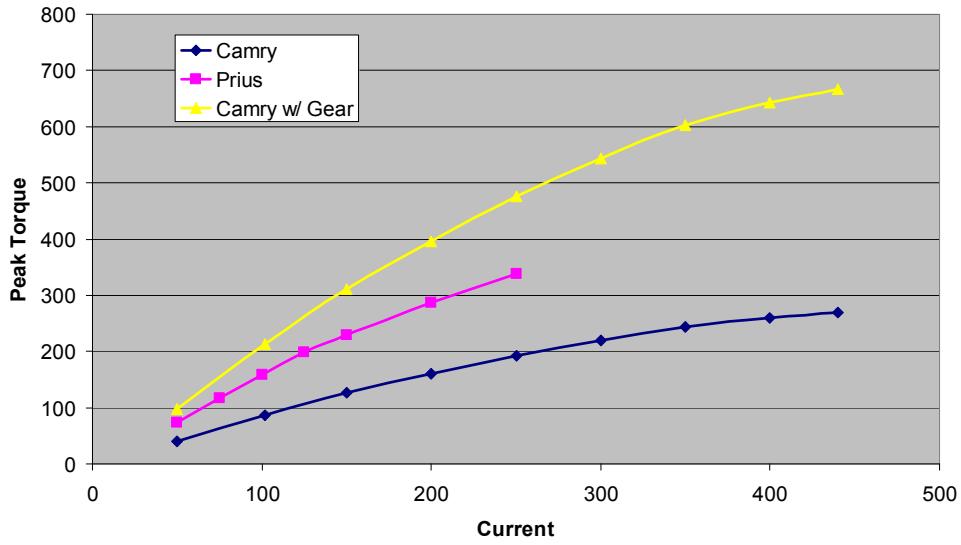

Fig. 3.15. 2007 Camry and Prius peak locked rotor torque vs. dc current.

Interior PM motors have two torque components and there is an optimal current angle at which the two torque components produce the maximum torque per current. Figure 3.16 shows the PM torque, reluctance torque, and the total sum of the two torque components for a constant exemplar current magnitude. Although the maximum PM torque is produced at a current angle of zero electrical degrees and the maximum reluctance torque is produced at 45 electrical degrees, the maximum total torque is produced at about 35 electrical degrees. This optimal current angle varies with many conditions such as current magnitude and speed.

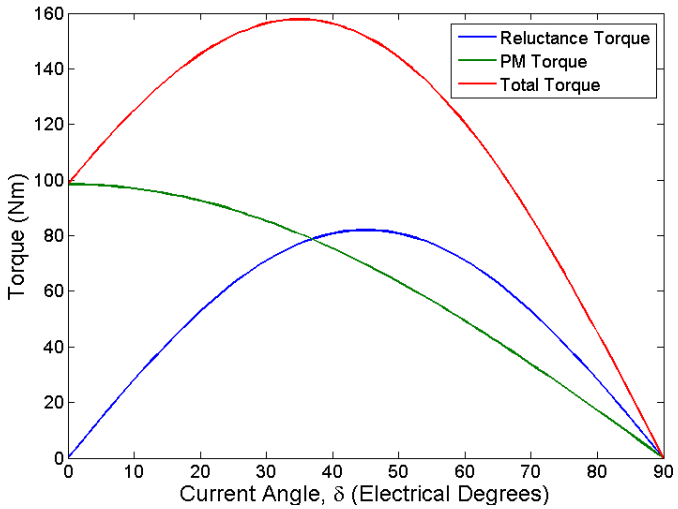

Fig. 3.16. 2007 Camry and Prius peak locked rotor torque vs. dc current.

3.5 PERFORMANCE AND EFFICIENCY EVALUATIONS

This section provides information about the performance and efficiency evaluations of the 2007 Camry hybrid subsystem components. The motor and inverter characteristics were evaluated simultaneously with power provided directly to the dc link as opposed to the power being supplied through the boost converter. Therefore, the 33 kW power rating of the inverter did not limit the capabilities of the motor and

inverter during the performance and efficiency assessment process. The dc-link voltage was maintained at 650 Vdc and a switching frequency of 10 kHz was used. Motor efficiency was measured throughout most of the entire torque-speed range in which the motor is capable of operating. For each operation point, the motor was controlled in steady state for at least 20 seconds and at least 5 data points were averaged to generate the efficiency map in Fig. 3.17.

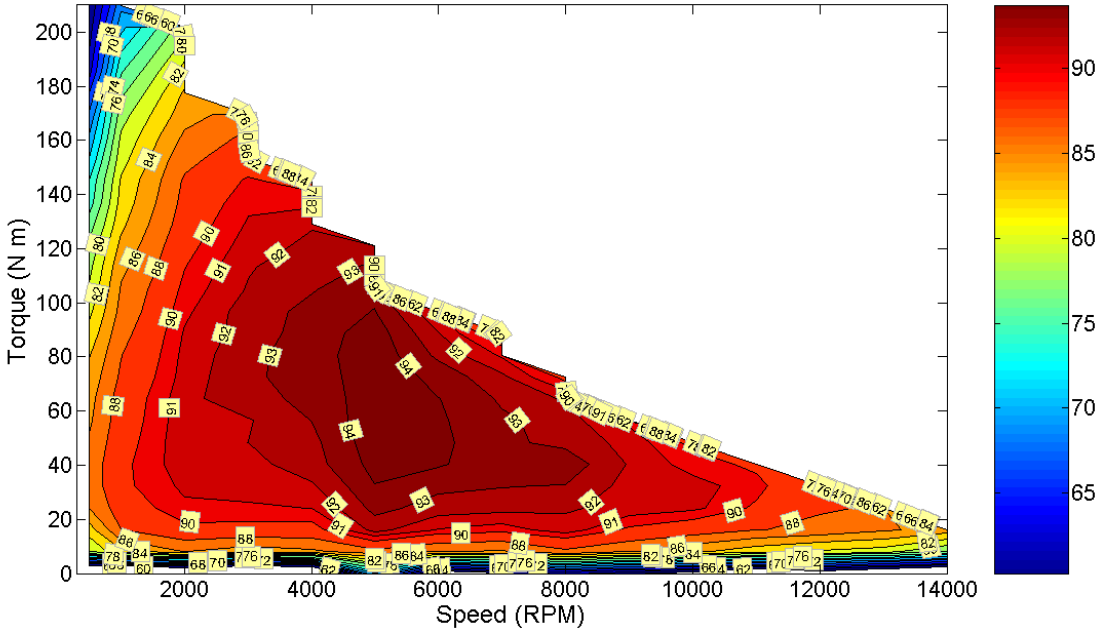

Fig. 3.17. 2007 Camry motor efficiency contours.

Efficiencies of the Camry motor are above 90% for a large portion of the torque-speed operation region. The high speed or high torque regions tend to incorporate lower operation efficiencies. To provide a straightforward comparison with the Prius motor efficiency map, the torque and speeds were scaled by 2.47 appropriately, as shown in Fig. 3.18. A comparison of the scaled Camry efficiency map and the Prius efficiency map in Fig. 3.19 reveals that the Camry has higher efficiencies for much of the map. Similar scales, axis limitations, percentage ranges, and color schemes are used to further ease the comparison. Note that a portion of the Camry high torque region is not visible. The most significant improvement over the Prius is observed at low speeds, where the Prius efficiencies drop quickly as torque increases and speed approaches zero. This region is frequented often since the electric motor is utilized to develop the torque required to accelerate the vehicle at low speeds or from standstill.

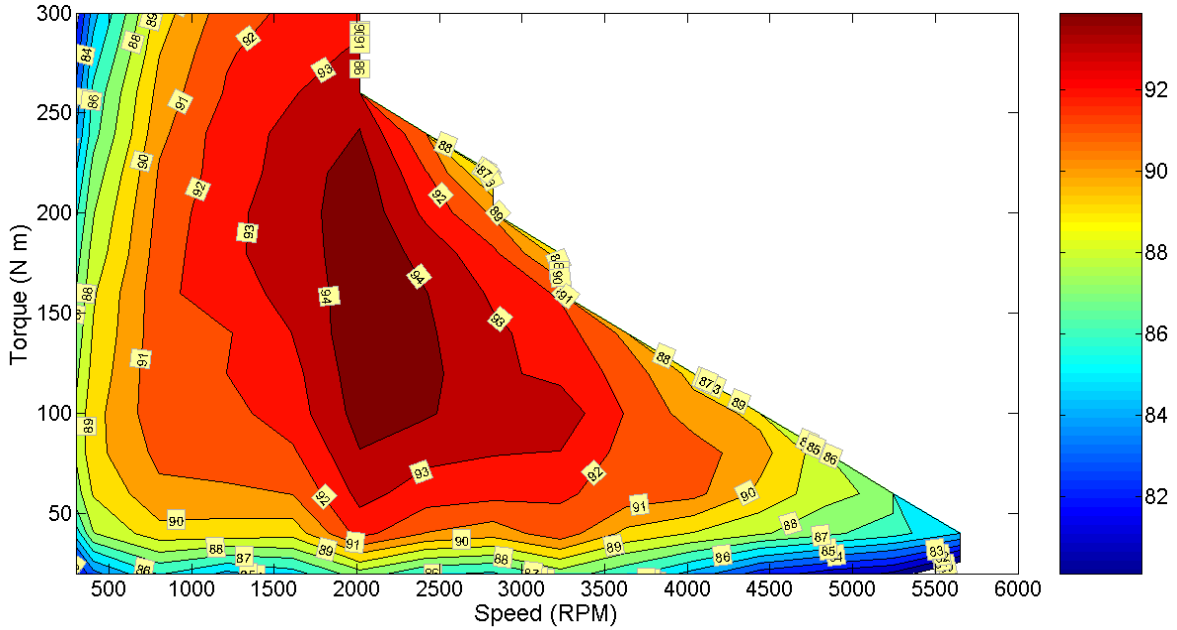

Fig. 3.18. 2007 Camry motor efficiency contours scaled by 2.47.

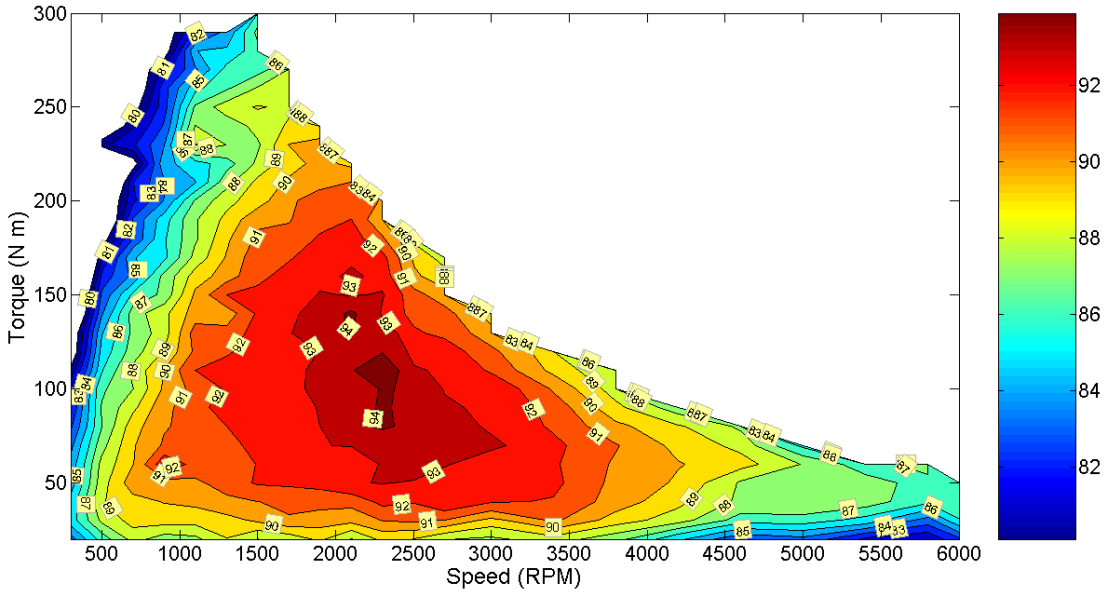

Fig. 3.19. 2004 Prius motor efficiency contours.

Thermal limitations hindered the extent of the Camry motor evaluations at low speeds and high torques, where steady state testing was limited to about 210 Nm in order to prevent over-temperature conditions. It has been verified through dynamic, short duration tests that the motor is capable of producing the published rated torque of 270 Nm, yet for only a very short time duration of a few seconds. According to the Camry service manual, the operation temperature of the motor is typically below 90ºC. With this limitation, the extent of maximum torque of 270 Nm is much shorter as temperature limitations were set at about 150ºC during the tests. The maximum power capability is limited by voltage constraints to about

70 kW at 4500 rpm. This matches the expected power rating based on the size of the generator inverter and boost converter. Estimated power rating techniques based on properties such as the mass, volume, speed, and thermal characteristics also result in similar power ratings for this motor. It is assumed that the published 105 kW power rating of the transaxle is the sum of the motor and generator power ratings as no rating is published for the generator.

Similar to the process used with the Camry motor efficiency contours, the Camry inverter efficiency contours were generated and scaled by the high speed gear ratio of 2.47 in order to provide a straightforward comparison with the Prius. A comparison of the inverter efficiency maps, shown in Figs. 3.20 and 3.21, indicates that the efficiency of the Camry inverter is somewhat lower than the efficiency of the Prius inverter for speeds below 2000 rpm. Similar scales, axis limitations, percentage ranges, and color schemes are used in these efficiency maps to further ease the comparison. The low speed, high torque capabilities of the Camry inverter appear to be greater than that of the Prius inverter as the speed reduction gear facilitates the use of a much lower current to generate the same amount of equivalent torque on the low speed side of the speed reduction gear. For low torques above 2000 rpm, the Camry inverter efficiency contours indicate that the efficiency decreases slightly as the torque approaches zero, whereas the Prius inverter efficiency remains consistent beyond 2000 pm. Higher losses of the Camry inverter is possibly due to the 30% increase of the dc-link voltage and the 50% increase in the number of power electronic devices when compared to that of the Prius.

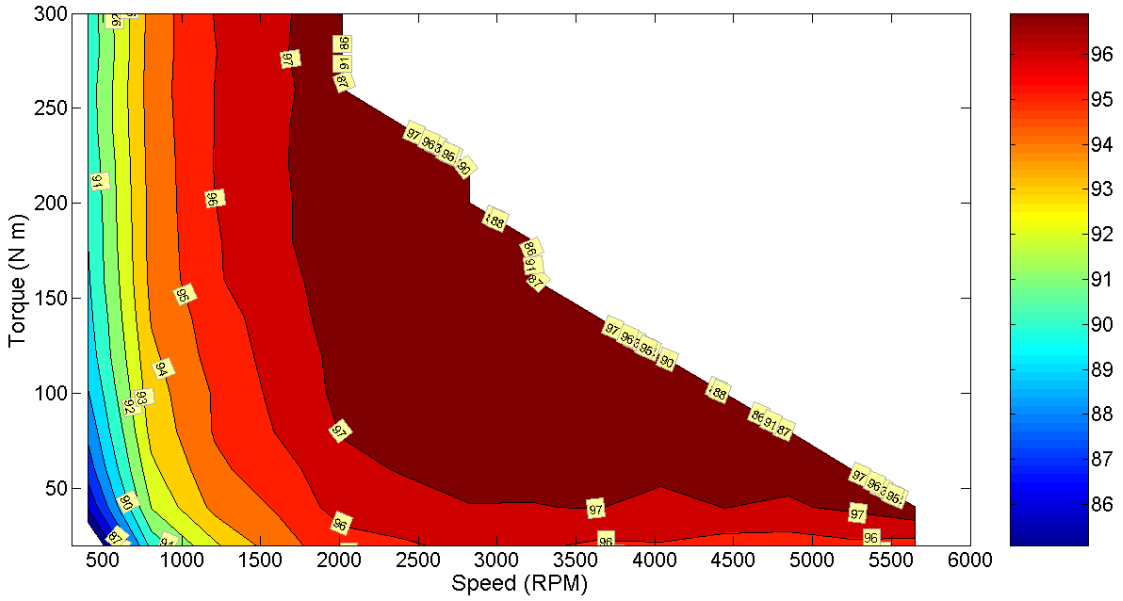

Fig. 3.20. 2007 Camry inverter efficiency contours scaled by 2.47.

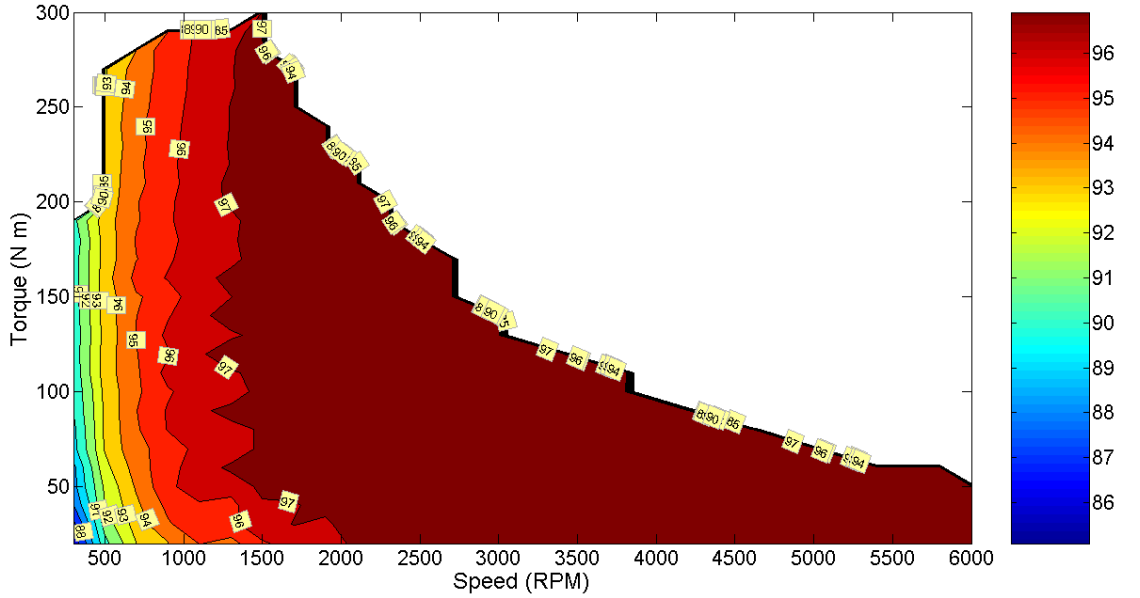

Fig. 3.21. 2004 Prius inverter efficiency contours.

The lower inverter efficiencies of the Camry cause the combined motor/inverter efficiencies to be somewhat closer than the motor efficiencies alone, as indicated in Figs. 3.22 and 3.23. Although there are striking similarities between the two efficiency contour maps, benefits of the high speed motor in the Camry are evident for the low speed, high torque regions.

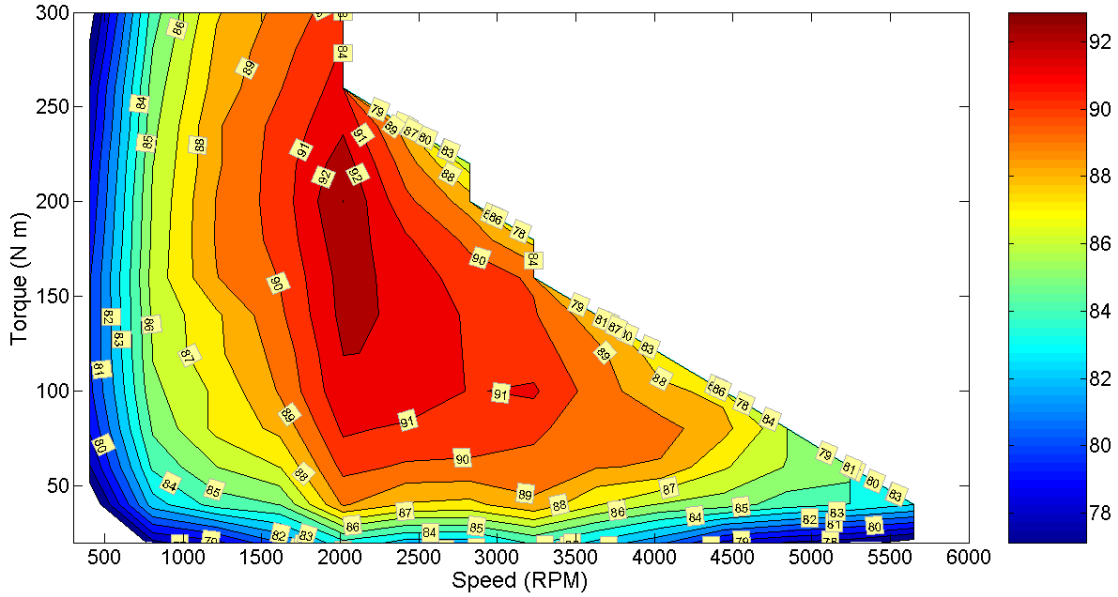

Fig. 3.22. 2007 Camry motor/inverter efficiency contours.

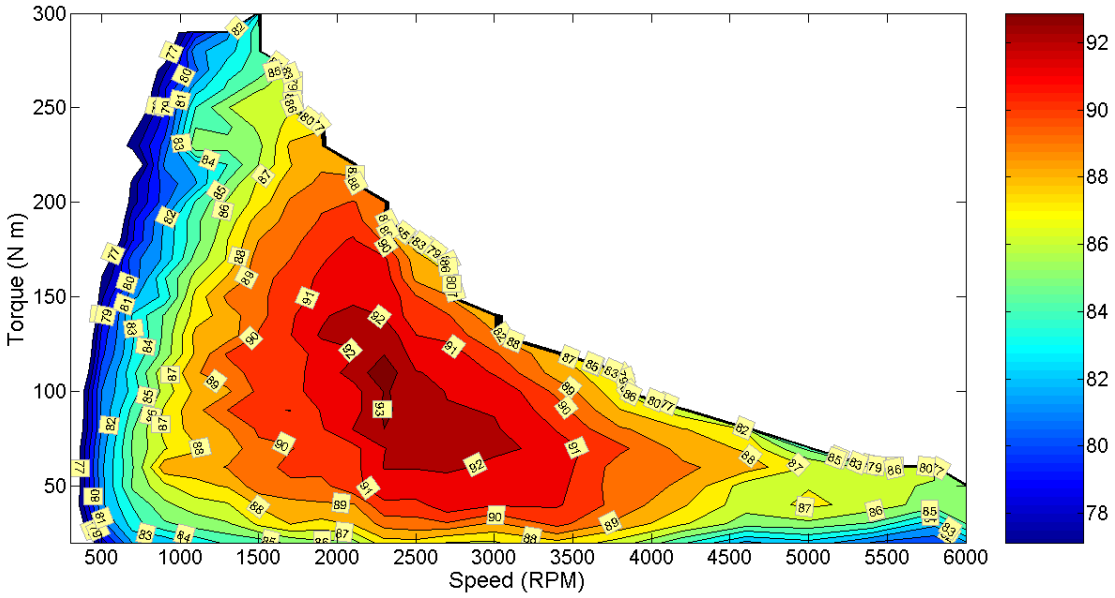

Fig. 3.23. 2004 Prius motor/inverter efficiency contours.

To further explore the various influences on inverter efficiency, tests were conducted with various dc-link voltages and inverter switching frequencies. In Fig. 3.24, a constant operation condition at 1000 rpm and 80 Nm was maintained throughout the tests. As expected, the inverter efficiency decreases with increasing dc-link voltage and increasing switching frequency. The Camry controller can operate at switching frequencies of 1.25 kHz, 2.5 kHz, 5 kHz, and 10 kHz, yet it operates at 5 kHz for much of the time when controlled by the MG ECU in vehicle. The impact of these parameters is lower for some operation conditions and high dc-link voltages are unavoidable at high speed, high torque conditions wherein back-emf voltages demand a high supply voltage.

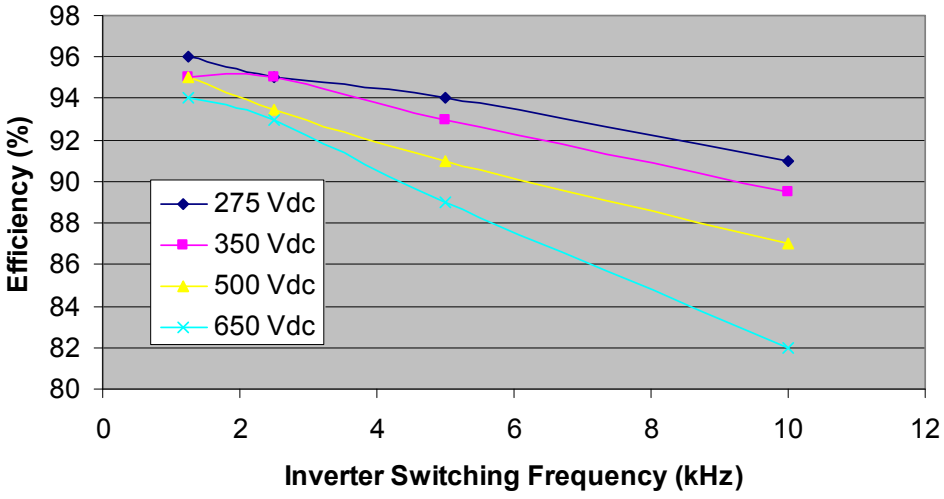

Fig. 3.24. 2007 Camry inverter efficiency vs. switching frequency for various dc-link voltages.

Boost converter efficiency assessments were conducted with various dc-link voltage and current output levels. The evaluations were conducted as the boost converter supplied the motor inverter, both of which

were operated at 5 kHz. The motor speed was maintained at 1000 rpm as the torque was increased to increase the boost converter current. According to the data from full vehicle tests conducted at ANL, the input voltage to the boost converter is commonly near 275 Vdc. Camry and Prius boost converter efficiencies are plotted versus boost converter input current in Figs. 3.25 and 3.26. Curve characteristics are undoubtedly different between the two, and the Prius boost converter has a slightly higher efficiency for much of the operation range. Low dc-current limitations were set for initial tests to prevent potential failures from preventing completion of general tests. Nonetheless, a failure occurred with an output voltage of 500 Vdc and input current of about 70 A and anticipated tests at 650 Vdc as well as a second series of tests at 10 kHz were not conducted. The failure was associated with an extremely high ripple current and the Toyota controller likely uses a switching frequency of 10 kHz in these conditions.

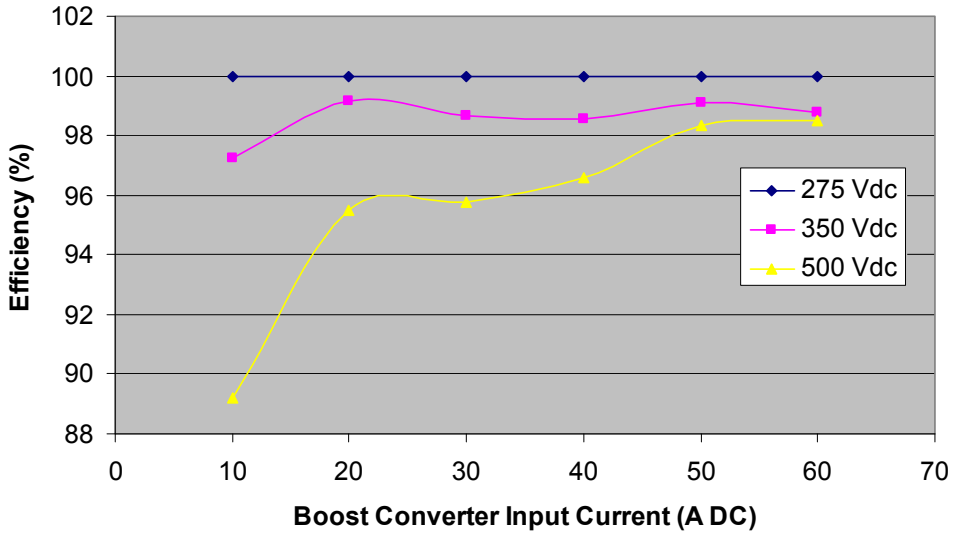

Fig. 3.25. 2007 Camry boost converter efficiency vs. input current for various dc-link voltages.

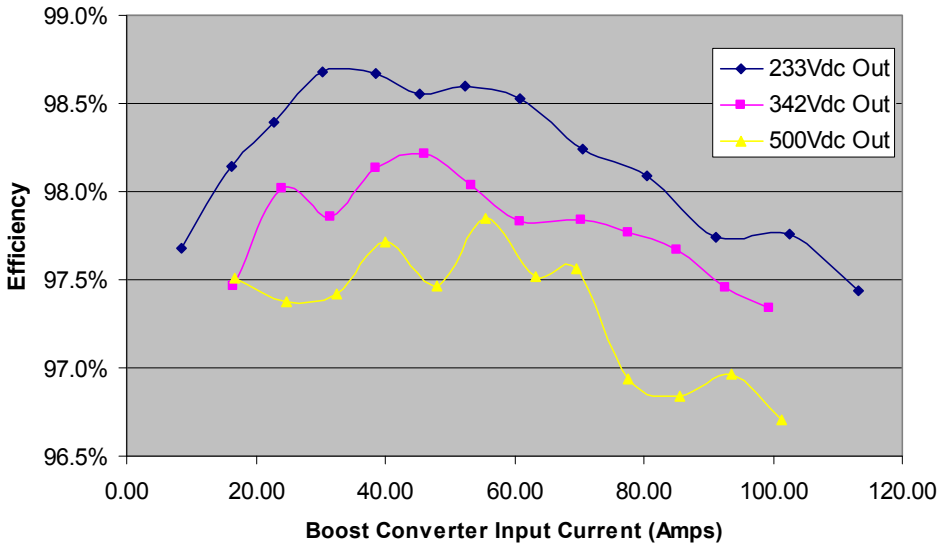

Fig. 3.26. Prius boost converter efficiency vs. input current for various dc-link voltages.

3.6 CONTINOUS LOAD DURATION TESTS

The Camry motor was operated at continuous power levels for different speeds and coolant temperatures to observe the continuous capability of the motor under various conditions. Continuous tests were conducted at 25, 33.5, and 50 kW at 3000, 5000, and 7000 rpm with coolant temperatures of 20, 25, 50, and 65ºC. For each case, motor temperatures were allowed to stabilize prior to initiating the continuous tests and the Bay-Voltex coolant temperature regulation unit was used to regulate the coolant at a desired temperature.

TCs and thermistors were installed in various locations throughout the transaxle and PCU with locations indicated in Fig. 3.5. Coolant temperatures are indicated by the traces labeled “To Camry” and “From Cam.” A thermistor labeled “D: ML 1” was installed within close proximity of the factory thermistor of the Camry, which is labeled “E: ML 2”. Additionally stator, internal/external case, and inverter temperatures were monitored and recorded.

Figure 3.27 shows the continuous test results conducted at a power level of 50 kW, a motor speed of 5000 rpm, and a coolant temperature of 50ºC. The traces are labeled and identified by color in the key provided on the left. Mechanical power, “Pmech,” is represented by a blue trace. The symbol at each datapoint is not distinguishable in the figure since the time scale is so large and the datapoints are close together. A table indicates the time duration for the associated stator temperature limitation in the upper left corner of the figure. For example, with a coolant temperature of 50ºC, the motor can operate at 50 kW for about 8:05 (minutes:seconds) prior to reaching a stator temperature of 130ºC. If the stator temperature limit is raised to 140ºC, the motor can operate for about 10:18 under these conditions. Thus, the extent of continuous operation capabilities depends greatly upon stator temperature limitations.

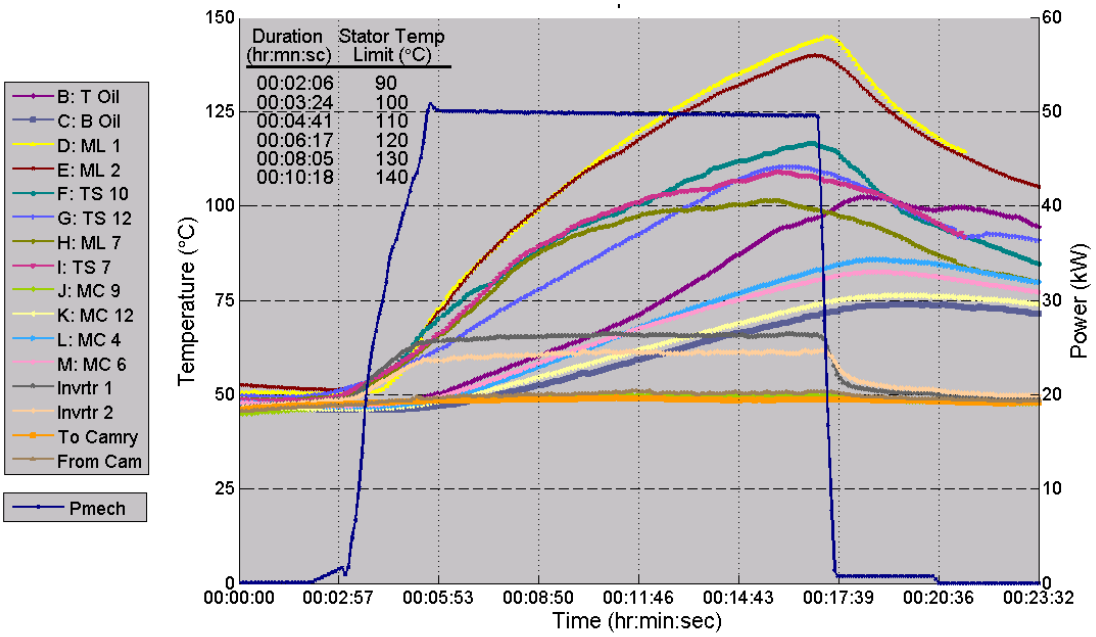

Fig. 3.27. Camry 50 kW continuous duration test at 5000 rpm with 50ºC coolant.

Stator temperature limitations are set to prevent potential damage within the stator windings and to prevent demagnetization of the PMs. Long term effects which affect the life of the PMSM must also be considered when choosing a stator temperature limitation. According to full vehicle tests at ANL, the Camry stator temperature is generally kept well below 90ºC. The temperatures of the original Camry

thermistor and the installed thermistor remained close during the continuous duration tests. Results show that the original Camry thermistor, "E: ML 2," is placed in one of the hottest locations of the motor. Figures 3.28 and 3.29 show the plots from tests conducted with a coolant temperature of 65ºC at power levels of 50 kW and 25 kW and 7000 rpm and 5000 rpm, respectively. Note that in the latter test the coolant temperature was reduced after thermal steady state was reached, as indicated in Fig. 3.29.

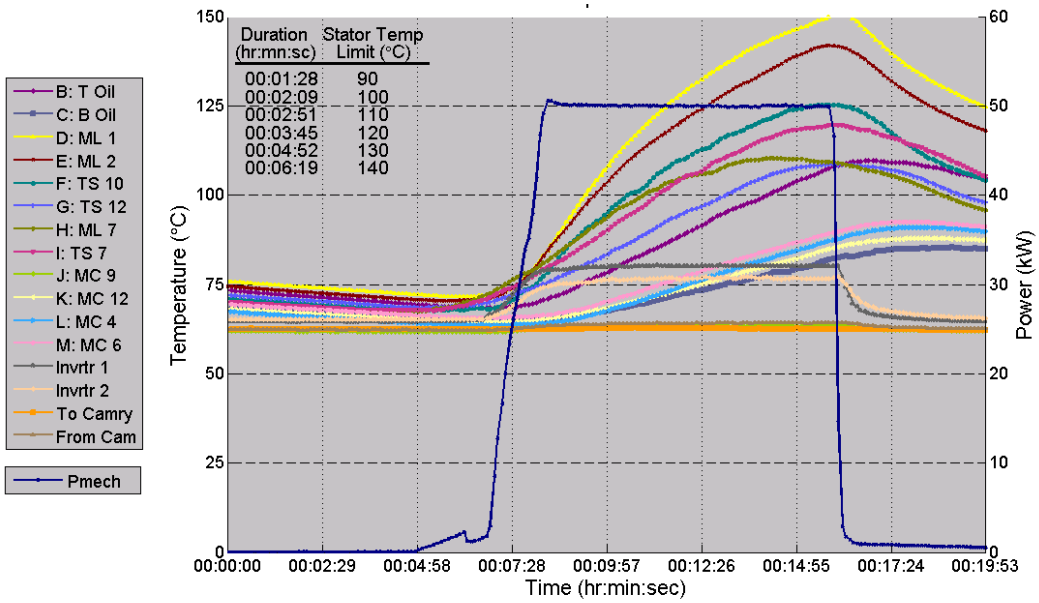

Fig. 3.28. Camry 50 kW continuous duration test at 7000 rpm with 65ºC coolant.

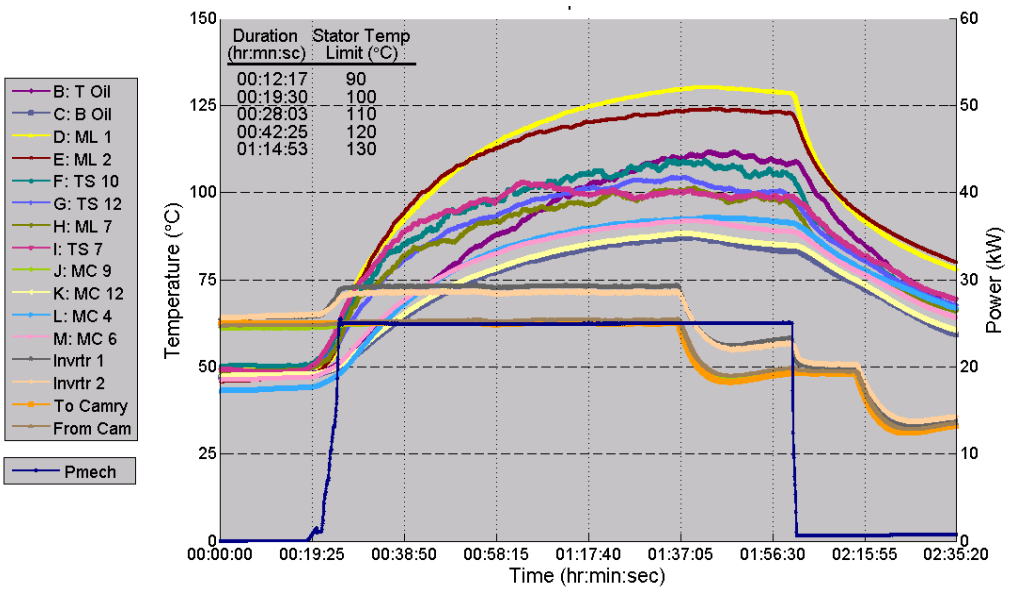

Fig. 3.29. Camry 25 kW continuous duration test at 5000 rpm with 65ºC coolant.

As expected, a comparison of Figs. 3.27 and 3.28 shows that the time extent of operation at 50 kW decreases as the test speed changes from 5000–7000 rpm and coolant temperature increases from 50–65ºC. All tests conducted at 5000 rpm produced the most efficient operation and thus the longest duration of operation at any power level when compared to test results obtained while operating at other

speeds and a similar coolant temperature. The highest temperatures stabilized near 130ºC in Fig. 3.29 at 5000 rpm and 25 kW. Note that it took over an hour to reach this temperature. Another continuous duration graph from tests conducted at 3000 rpm and 33.5 kW with a coolant temperature of 65ºC is shown in Fig. 3.30.

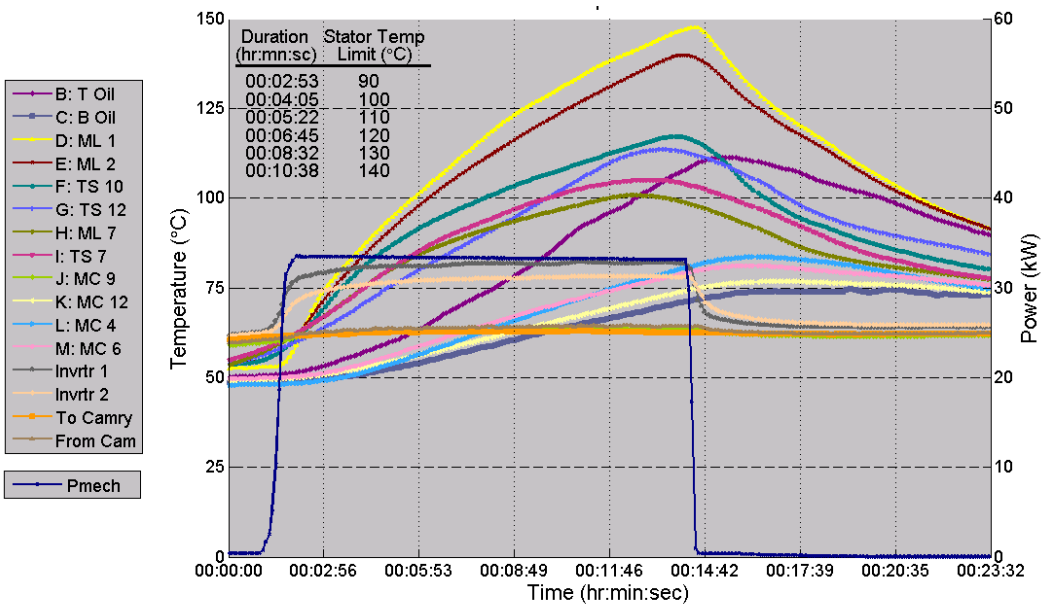

Fig. 3.30. Camry 33.5 kW continuous duration test at 3000 rpm with 65ºC coolant.

Graphs similar to Fig. 3.30 were generated for each test condition and while they are informative, it is difficult to fully study the impact of various power levels, motor speeds, coolant temperatures, and stator temperature limitations upon the extent of time at which the motor can operate under these conditions. Therefore, the duration times shown in the upper left corner of the previous figures were used to produce graphs which provide more meaningful comparisons. In Fig. 3.31, the time durations associated with operation at 25 kW with a 65ºC coolant temperature is graphed versus speed. Each trace represents the time durations which correlate to a particular stator temperature limit. Through inspection of this graph, it is more evident that the duration of operation is greater at 5000 rpm than for any other speed. Note again that in this case, the stator temperature stabilized near 130ºC at 5000 rpm, which is represented by the upper most trace. Thus, the trace for a temperature of 150ºC would theoretically have a data point that approaches infinity. Also note that tests under these conditions were discontinued after 30 minutes of operation at 7000 rpm and therefore stator temperatures did not reach higher than 120ºC.

Similar graphs are shown in Fig. 3.32 for a power level of 33.5 kW and a coolant temperature of 35ºC. At 5000 rpm, the motor operated for over 30 minutes before reaching a stator temperature of 125ºC. For low stator temperature limits, the duration capability does not change significantly as the motor speed increases from 5000–7000 rpm.

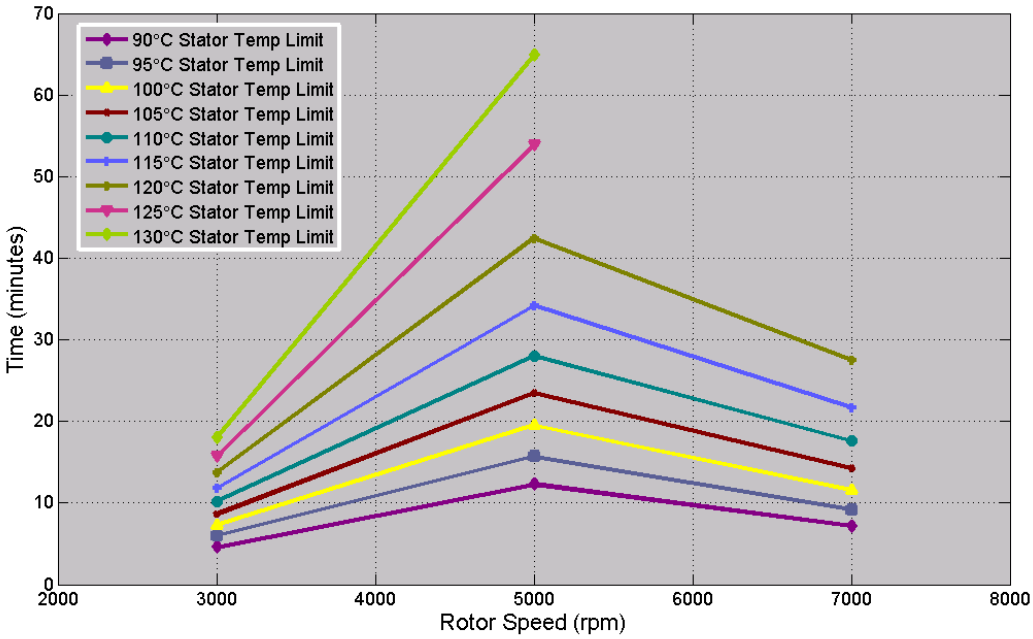

Fig. 3.31. Camry 25 kW continuous duration vs. speed with 65ºC coolant.

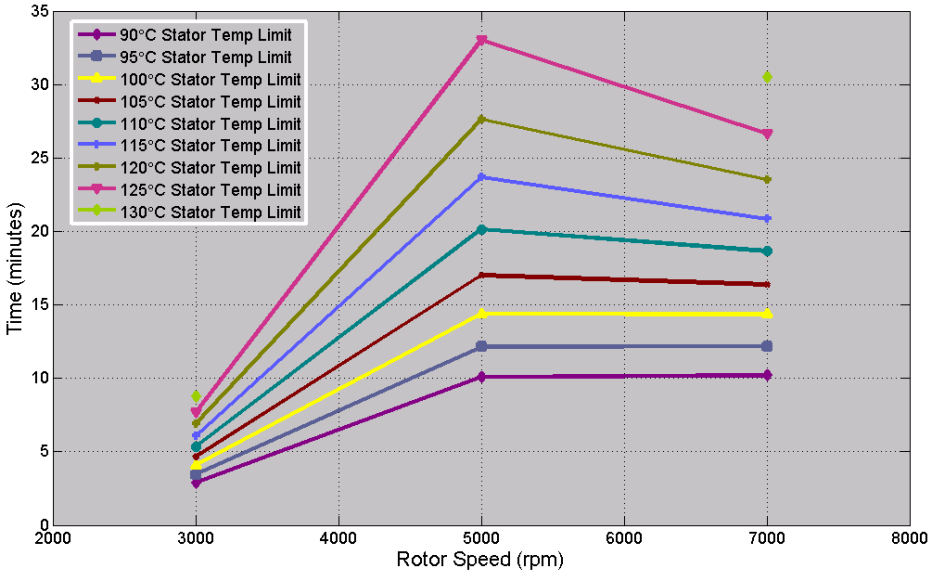

Fig. 3.32. Camry 33.5 kW continuous duration vs. speed with 35ºC coolant.

Similar graphs are shown in Figs. 3.33 and 3. 34 for continuous tests conducted at 50 kW with coolant temperatures of 35ºC and 65ºC, respectively. The trace color and stator temperature limitation correlations are consistent for all of the graphs to provide ease in comparisons. The impact of coolant temperature is quite visible as the time for stator temperatures to reach 135ºC at 5000 rpm is about 13 minutes with a 35ºC coolant temperature versus about 8 minutes with a 65ºC coolant temperature.